UNIVERSITAT ROVIRA i VIRGILI

UNVEILING THE ROLE OF OXIDIZED MYELIN DEBRIS IN BV-2 MICROGLIA: INSIGHTS INTO MULTIPLE SCLEROSIS

TREBALL DE FI DE GRAU

MARTA SANTACREU VILASECA

TUTORA ACADÈMICA: ANNA MAS

BIOQUÍMICA I BIOLOGIA MOLECULAR

TARRAGONA, 2023

INDEX

1. ABSTRACT

Multiple sclerosis (MS) is an autoimmune inflammatory neurodegenerative disease in which the immune system attacks the myelin sheath that covers nerve fibers. This immune attack leads to an inflammatory environment with an increased presence of reactive oxygen species (ROS), potentially causing oxidative stress and resulting in neuronal deterioration, leading to permanent damage. During this immune attack, myelin debris is generated and must be phagocytosed by microglia. Given that this myelin debris is present in an oxidative environment, it is hypothesized that it tends to undergo oxidation. In this investigation, the consequences of microglial phagocytosis of said oxidized debris were analyzed using the murine microglial cell line BV-2. Differential exposure to normal and oxidized myelin debris was employed to assess their impact on cellular viability, protein biosynthesis, and the expression of inflammatory cytokines. Additionally, the phagocytic process was examined by staining myelin with the CFSE reagent, considering both treatment variations and their duration. The results of this study demonstrate mar ked disparities in various proteins related to the antioxidant cell capacity and cellular metabolism, alongside a significant distinction in phagosomal degradation engendered by oxidized myelin when juxtaposed against control myelin. These findings suggest that the oxidation of myelin disrupts the physiological and pathological functions of microglia, thereby suggesting it as a compelling target for future investigations.

2. INTRODUCTION

Multiple Sclerosis (MS) is a chronic inflammatory neurological disorder that profoundly affects the central nervous system (CNS) [1]. It is characterized by an autoimmune response in which the immune system erroneously targets and damages the myelin sheath, a protective layer encompassing and insulating nerve fibers in the CNS, leading to demyelination and axonal degeneration. The resultant damage disrupts the transmission of nerve impulses, giving rise to a diverse array of symptoms encompassing muscle weakness, balance and coordination impairments, fatigue, visual impairment, cognitive deficits, and sensory disturbances [2].

MS stands as one of the most prevalent neurological conditions worldwide and, in numerous countries, ranks as the foremost cause of non-traumatic neurological disability among young individuals aged 20 to 40 years, affecting females approximately twice as frequently as males. Globally, it is estimated that MS afflicts 2.8 million individuals, corresponding to a prevalence of approximately 1 in 3,000 people. This figure has increased since 2013, when the estimated number of affected individuals stood at approximately 2.3 million. While several factors may have contributed to this rise, such as improved diagnostic methodologies and extended life expectancy

among MS patients, the possibility of a substantial elevation in the risk of developing MS cannot be dismissed [3].

This disease can progress in various ways: The Clinically Isolated Syndrome (CIS) describes the first clinical event highly suggestive of demyelinating CNS disease but not yet meeting the necessary criteria, for the diagnosis of clinically definitive MS (CDMS). Like in other MS attacks, the episode is expected to last at least 24 hours (in the absence of fever or infection). Although this type of episode is a hallmark of MS, it is noteworthy that not all individuals with CIS inevitably transition to a definitive diagnosis of MS [4, 5]. The term RRMS (relapsing-remitting multiple sclerosis) describes the most common phenotype found in approximately 85% of MS patients. It is characterized by alternating periods of neurological dysfunction, known as relapses, and periods of relative clinical stability without new neurological symptoms, referred to as remissions. The frequency of relapses can vary among patients but generally does not exceed 1.5 per year. During a relapse, individuals may experience a range of neurological symptoms, including but not limited to weakness, changes in sensation, difficulties with balance, and impaired visual acuity. These symptoms persist for a minimum of 24 hours. Almost half of the relapse episodes result in residual deficits, leading to a gradual accumulation of impairment. Recovery of symptoms during relapse resolution suggests remyelination, which is most active during the early inflammatory phase of MS [4]. Most untreated patients RRMS ultimately transition to secondary progressive multiple sclerosis (SPMS). The diagnosis of SPMS is typically retrospective, often occurring years after the actual onset of progression. [4]. SPMS is characterized by a continuous progression, with or without occasional relapses, minimal significant remissions, and stability phases [6,7]. Finally, there is the Primary Progressive MS (PPMS) characterized by a progressive decline in neurological function that leads to the accumulation of disability from the onset of symptoms, without the occurrence of early relapses or remissions. A key feature that sets PPMS apart from other disease courses, is the significantly lower levels of inflammation associated with PPMS. Consequently, individuals with PPMS often exhibit fewer brain lesions, although they tend to have a higher prevalence of lesions in the spinal cord compared to the brain [5].

2.1 Etiology of MS

MS is widely regarded as a multifactorial disorder influenced by both genetic and environmental factors. Extensive genomic investigations have identified more than 200 gene variants associated with a predisposition to MS [8]. Among these variants, the major histocompatibility complex alleles, particularly the HLA-DRB1 allele, exhibit the most significant association with the disease, carrying the highest risk. The majority of MS risk alleles are intricately linked to the immune system, underscoring the pivotal role of immunogenetics in the pathogenesis of MS. Nonetheless, genetic factors alone account for only approximately 30% of the explained risk of suffering MS, with environmental factors assuming considerable prominence. These environmental factors include low levels of vitamin D, obesity, smoking, and infections, notably those involving the Epstein-Barr virus [9].

Regarding the immune system's involvement, it is postulated that the initiation of MS pathology originates from the activation of T cells that exhibit reactivity against the central nervous system (CNS) within the peripheral immune system. Two primary hypotheses (*figure 1*) have been proposed to elucidate this phenomenon: (a) cross-reactivity with foreign antigens and (b) recognition of CNS-derived antigens that have permeated the cervical lymph nodes. The former hypothesis suggests that antigen-presenting cells (APCs) capture foreign antigens, subsequently migrating through the lymph node drainage system and potentially activating T cells that cross-react with self-antigens from the CNS. Following their activation and polarization toward proinflammatory phenotypes, these self-reactive T cells migrate to the CNS. The latter hypothesis suggests that soluble CNS antigens present in the cerebrospinal fluid can activate T cells within the cervical lymph nodes. Notably, an important feature shared with other autoimmune diseases is the expansion of epitopes in MS, whereby the immune response directed against one epitope extends to other epitopes, either within the same antigen or across different peptides, thereby intensifying the autoimmune pathogenic response. [9, 10]

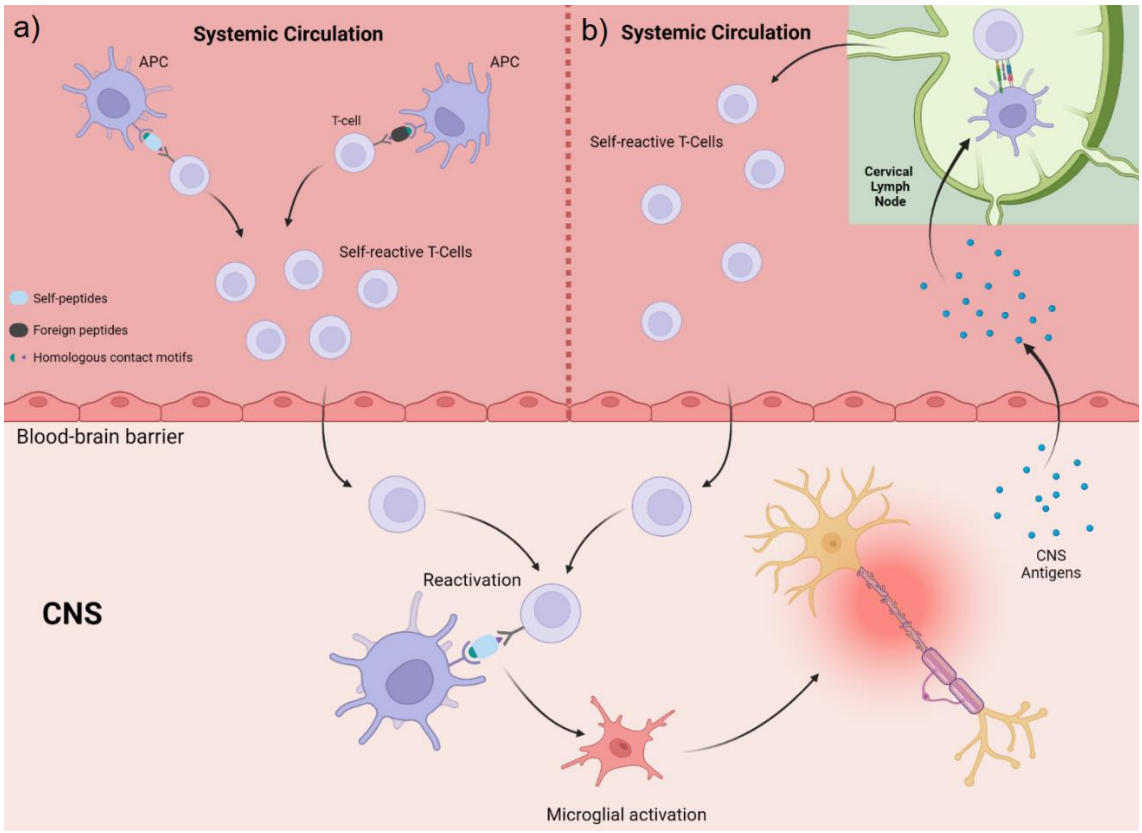

Figure 1. The depiction illustrates the two primary hypotheses of T cell activation in MS. **A.** Cross-reactivity with external antigens. **B.** Recognition of CNS-derived antigens that have infiltrated the cervical lymph nodes.

In considering the migration of T cells to the CNS, it is crucial to acknowledge the presence of the blood-brain barrier (BBB), which serves as a selective barrier limiting the transit of circulating cells and large molecules. This unique feature endows the CNS with immunological privilege. Consequently, activated T cells must traverse the BBB to exert their damaging effects within the CNS. Although the precise mechanisms guiding the migration of these cells to the CNS remain unclear, it is posited that the activation of T cells prompts the expression of molecules that facilitate their internalization by CNS endothelial cells. Additionally, observations indicate that damaged tissues in proximity to CNS lesions exhibit enhanced expression of chemokines by endothelial cells, thereby promoting the activation of integrins responsible for immune cell infiltration. Noteworthy endothelial adhesion molecules, such as intracellular adhesion molecule 1 (ICAM-1), vascular cell adhesion molecule 1 (VCAM-1), and E-selectin, are prominently upregulated in MS lesions. [9]

Once infiltrated within the CNS, autoreactive cells undergo reactivation mediated by microglia, dendritic cells, and other resident CNS cells. This reactivation process is essential for the progression of pathology within the CNS [11]. Notably, a distinctive characteristic of MS is that

patients often experience partial or complete recovery following the initial manifestation of symptoms. This phenomenon can be attributed to diverse anti-inflammatory physiological mechanisms, including the apoptosis of inflammatory cells and the production of anti-inflammatory cytokines by the CNS. It is believed that these cytokines act on lymphocytes and APCs to suppress inflammation, while microglia fulfill a role in eliminating cellular debris and dead cells. Moreover, although most lesions exhibit signs of remyelination subsequent to the destruction of myelin and axons, oligodendrocytes only partially remyelinate the damaged axons, thus failing to fully restore the original myelin thickness [9].

2.2 Pathology of MS

Progressive forms of MS encompass numerous pathological characteristics shared with the more prevalent recurrent variants. While localized inflammatory lesions within the white matter represent a distinctive hallmark of recurrent MS, progressive disease processes manifest a more intricate pathology entailing diverse pathways and mechanisms. Many of these mechanisms are inherent to both progressive and recurrent MS, displaying relative rather than absolute distinctions. Broad-ranging mechanisms encompass inflammation, axonal degeneration, microglial activation, mitochondrial impairment, accumulation of reactive oxygen species (ROS), and glutamate excitotoxicity.

Axonal degradation and its subsequent loss occur through various mechanisms (*figure 2)*, encompassing anterograde and retrograde injury, as well as trans-synaptic degeneration distant to areas of axonal transection. Axonal impairment arises in intact axons as a consequence of energetic/metabolic breakdown prompted by compensatory mechanisms aimed at preserving nerve impulse conduction following demyelination. These mechanisms entail an upregulation and reorganization of sodium channels. Constrained energy reserves results in depletion of the sodium/potassium ATPase activity, this coupled with subsequent sodium accumulation within the axon, elicit activation of the sodium/calcium transporter, facilitating calcium influx into axons, and ultimately precipitating secondary neurodegeneration and axonal loss [12]. Microglial activation arises as a consequence of demyelination and oligodendrocyte renewal subsequent to oxidative lesion development. The precise role of microglia in neurodegeneration, whether beneficial or detrimental, remains a subject of extensive debate. Following demyelination, microglia assume crucial functions in the phagocytic elimination of myelin debris. Moreover, they secrete diverse growth factors that facilitate the regenerative process, alongside compounds implicated in the survival, proliferation, differentiation, and maturation of oligodendrocytes, the key players in myelogenesis [13]. Activation of microglia leads to increased production of ROS and nitric oxide,

producing a potentially toxic environment for axons. Additionally, microglia plays a role in augmenting immune activation through antigen presentation. Oxidative damage is amplified by the accumulation of iron, which is released by oligodendrocytes and sequestered by microglia, typically at the periphery of lesions and within deep gray matter structures. [12, 13]

Demyelination instigates mitochondrial dysfunction and leads to mitochondrial/nuclear DNA mutations. This mitochondrial dysfunction renders axons particularly vulnerable to oxidative damage, and the resultant surge in oxidative byproducts subsequently exacerbates mitochondrial dysfunction, perpetuating a self-amplifying cycle. Anomalous displacement of mitochondria within demyelinated axons provokes energy deficits and limited energy availability, ultimately culminating in axonal degeneration [12]

Elevated glutamate production by microglia has also been observed as a consequence of ROS accumulation. Excessive glutamate levels can induce injurious effects on myelin directly and disrupt calcium homeostasis within axons and oligodendrocytes, giving rise to a detrimental feedback loop involving glutamate overload and increased production of oxidative substances [12].

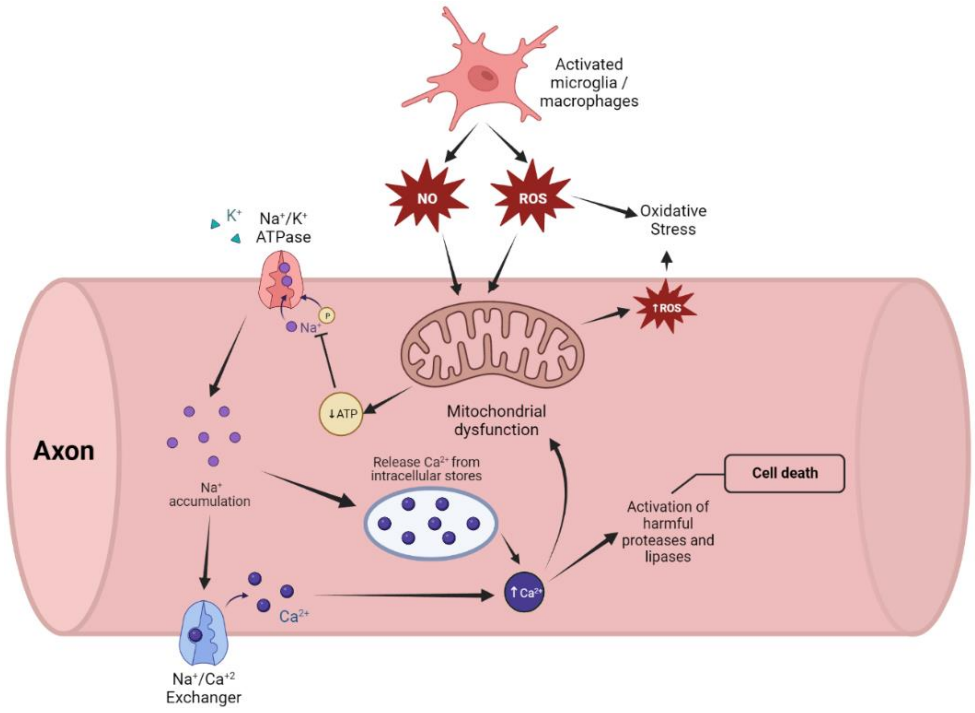

Figure 2. Depiction of the summarized process in which the generation of ROS and NO by activated microglia leads to mitochondrial dysfunction, resulting in a reduction of energy production, an increase in oxidative stress, and ultimately leading to sodium and calcium accumulation, axonal damage, and cell death.

2.3 Treatment of MS

There is currently no known cure for MS; however, therapeutic interventions exist that can mitigate the frequency and severity of relapses, thereby delaying the progression towards long-term disability [14]. In acute relapses, the primary therapeutic approach revolves around the administration of corticosteroids, owing to their potent anti-inflammatory and immunosuppressive properties [15]. Methylprednisolone is generally administered intravenously, although it has been shown to have similar efficacy when taken orally [16]. Numerous investigations have shown that these pharmacological agents expedite the recovery from MS attacks, yet they do not alter the long-term trajectory of the disease [14]. Alternative options for managing acute relapses encompass adrenocorticotropic hormone [16] and plasma exchange (plasmapheresis), with the latter being reserved for instances of MS that exhibit an inadequate response to methylprednisolone. Nevertheless, this particular therapeutic modality has demonstrated limited efficacy in individuals presenting with SPMS or PPMS. [14].

There are also disease-modifying treatments (DMTs) available. The selection of the administered agent is based on patient-specific factors and the trajectory of the disease. It is imperative that a neurologist oversees this form of treatment, and it is crucial to note that only one therapeutic agent should be utilized at a time, as there has been no observed efficacy in combining these treatments. Particularly, these interventions exhibit effectiveness, in the initial stages of the disease, targeting RRMS and SPMS. Regrettably, no existing agents sufficiently address CIS, and the available options for primary progressive multiple sclerosis PPMS are notably limited [16].

Injectable medications encompass a class of DMTs, one of the widest employed pharmacological strategies in MS treatment is 9 interferon drugs. These medications assume a pivotal role in regulating immune cells, reducing inflammation, and preventing nerve damage. They present adverse effects, such as flu-like symptoms (typically mitigated with ongoing therapy), depressive episodes, and elevated hepatic enzyme levels. In certain cases, the therapeutic effect may diminish following 18-24 months of treatment, necessitating a change in medication. Another injectable option, glatiramer acetate, modulates immune cells within the body, although the precise underlying mechanism is not fully understood [16].

Shifting the focus to infusion therapeutic modalities, a noteworthy category comprises monoclonal antibodies, such as Natalizumab, which impedes the migration of immune cells across the blood-brain barrier into the central nervous system. While highly effective, Natalizumab

carries an elevated risk of progressive multifocal leukoencephalopathy (PML), a potential viral infection within the brain. Consequently, this treatment is exclusively recommended for individuals unresponsive to the aforementioned first-line therapies. Ocrelizumab is an alternative approach to treating relapsing forms of PPMS in adult patients. This medication targets circulating immune cells and carries a higher risk of cancer and infections as a side effect. Alemtuzumab, an additional alternative, selectively targets surface proteins on immune cells. However, due to its potential to trigger autoimmune diseases, its usage is not recommended unless alternative therapies have proven ineffective [14].

Finally, within the realm of infusion treatments, we encounter mitoxantrone, an inhibitor of topoisomerase II that obstructs the cellular replication process. Reserved exclusively for severe cases of RRMS and SPMS, mitoxantrone's potential side effects encompass the development of specific blood cancer and cardiac damage. Consequently, it serves as a last resort for patients experiencing a rapid decline in functional capacity as a result of their MS progression, with no response to alternative treatments [14, 17].

For oral disease-modifying therapies DMTs, we have Fingolimod, which is administered on a daily basis and demonstrates efficacy in reducing relapses among both adult and pediatric patients. This pharmacological agent exerts its therapeutic effect by the lymphocytes from leaving the lymph nodes and their subsequent infiltration into the systemic circulation, as well as CNS. Nonetheless, it is noteworthy that Fingolimod administration may induce bradycardia and ocular complications, while concomitantly elevating the susceptibility to infections. Another oral DMT available is dimethyl fumarate, which is indicated for the management of relapsing forms of MS. Despite its established clinical efficacy, the precise mechanism underlying its therapeutic action remains unknown, and adverse effects such as lymphopenia, nausea, and gastrointestinal disturbances have been reported. Alternatively, diroximel fumarate represents a viable treatment option, exhibiting similarities to dimethyl fumarate, yet manifesting a reduced propensity for gastrointestinal side effects. Diroximel fumarate is specifically designed for individuals with SPMS, it is believed to reduce brain and spinal cord damage reducing CNS inflammation by modulating immune responses. Teriflunomide constitutes yet another oral DMT, acting by inhibiting the proliferation of activated immune cells. Notwithstanding its favorable therapeutic attributes, teriflunomide may give rise to adverse reactions including nausea, diarrhea, hepatotoxicity, and alopecia. Moreover, Cladribine therapy offers an alternative approach by targeting lymphocytes involved in immunological assaults within the context of MS. It should be underscored, however, that cladribine utilization is associated with an augmented likelihood of cancer development,

warranting its consideration as a final-line treatment strategy. Lastly, Siponimod tablets, exhibiting a mechanism of action akin to that of fingolimod, and they are indicated for the treatment of SPMS. Clinical trials have conclusively demonstrated that cladribine, diroximel fumarate, and dimethyl fumarate confer a reduction in relapse rates, delay the progression of disability, and mitigate the development of cerebral lesions. In addition to the aforementioned therapeutic interventions, comprehensive management of MS necessitates the effective addressing of associated symptoms encompassing visual impairments, muscular weakness, tremors, fatigue, pain, and numerous other manifestations [14]. As previously mentioned, the pathogenesis of MS encompasses the involvement of microglia in both advantageous and detrimental capacities. This particular cell type assumes a substantial role in the pathological mechanisms affecting both white and gray matter. Demyelination, which impacts both components, can be counteracted through remyelination, a process in which microglia actively participate by releasing cytokines that facilitate the preservation and maturation of oligodendrocyte progenitors responsible for myelogenesis [13, 18]. Nonetheless, gray matter neurodegeneration is irreversible and manifests early in the course of MS, standing as the primary etiology of enduring disability. This aspect becomes even more relevant when considering the limited efficacy of current disease-modifying treatments (DMTs), which solely mitigate the loss of white matter and offer restricted properties in attenuating or preventing gray matter neurodegeneration [19].

3. HYPOTHESIS AND OBJECTIVES

The hypothesis underlying this study posits that under oxidative conditions, the myelin debris generated by the immunological attack undergoes oxidation, potentially impairing the phagocytic capability of microglia cells. Consequently, it is anticipated that the *in vitro* treatment of microglia cells with diverse concentrations of unoxidized and oxidized myelin debris will yield noteworthy disparities in protein expression profiles and the cells' phagocytic functionality. Based on this premise, the primary objective of the present study is to probe into these conceivable alterations, aiming to appraise the viability of BV-2 cells as an in vitro model for scrutinizing MS, taking into consideration the oxidative milieu of the immune lesion and the presence of oxidized myelin debris. Thus, in order to achieve this primary objective, the following secondary objectives were formulated.

- Investigate the phagocytic response in microglial cells.
- Evaluate the detrimental effects of oxidized myelin and the subsequent response on microglia.
- Study the expression of inflammatory mediators in microglia in response to exposure to oxidized myelin debris.

- To investigate and assess the potential suitability of BV-2 cells as a experimental model for evaluating the efficacy of various treatments.

4. MATERIALS AND METHODS

4.1 BV-2 Cell Line

The BV-2 cell line is an immortalized cell line derived from microglial cells obtained from C57/BL6 mice. This cell line, commercially obtained from *AcceGen Biotech (Cat ABC-TC212S)*, exhibits a remarkable capacity for proliferation and metabolic activity, surpassing that of other microglia. Despite this heightened activity, the BV-2 cell line faithfully maintains the functional and morphological characteristics of microglia. In fact, it shares notable similarities with macrophages, such as their phagocytic capacity, antimicrobial activity, and antigen profile. Additionally, like other microglia, this cell line can be activated to release pro-inflammatory cytokines when exposed to inflammatory factors or oxidative stress. Consequently, the BV-2 cell line serves as an outstanding alternative model system for investigating primary microglia and studying neurodegenerative diseases *in vitro*. [20]

4.2 Extraction, Oxidation, and Labeling of Myelin Debris

4.2.1 Extraction and Oxidation of Myelin Debris

The myelin debris was extracted according to the protocol described by [21], with some modifications. Tris·Cl Buffer solution was prepared by adding 20 mL of 1 M Tris·Cl and 20 mL of 100 mM Na2EDTA to 800 mL of distilled deionized water (ddH_2O). The pH was then adjusted to 7.45, and the total volume was brought up to 1 L. This was utilized to prepare two sucrose solutions: one with a concentration of 0.32 M and the other with a concentration of 0.83 M.

The next step was euthanizing six mice, extracting their brains, and submerging them in 30 mL of the 0.32 M sucrose solution. Using a sterile hand-held rotary homogenizer, the brains were thoroughly homogenized. The homogenized brain solution was brought to a final volume of 90 mL by adding the 0.32 M sucrose solution. Ultracentrifuge tubes were loaded with 20 µL of the 0.83 M sucrose solution, onto which the homogenized brain solution was gently layered to create a density gradient. These tubes were then subjected to a centrifugation process, set at 100,000 x g for 45 minutes at a constant temperature of 4 ºC, employing minimal acceleration and deceleration. As a result, the myelin formed a visibly distinct whitish interface, which was collected and transferred to a 50 mL tube. The volume was adjusted to 35 mL using Tris·Cl Buffer to ensure thorough and effective mixing. The suspension was homogenized once again. The centrifugation process was repeated, this time utilizing the maximum acceleration and deceleration settings, to effectively precipitate the myelin debris. The supernatant was discarded, leaving behind a pellet

of myelin debris. This pellet was then resuspended in 10-15 mL of Tris·Cl solution. To further enhance the purification, the myelin was subjected to another round of centrifugation under the exact same conditions, resulting in a pellet that was subsequently resuspended in 5-6 mL of sterile HBSS, ensuring optimal purity.

The myelin debris suspension was divided among several pre-weighed 1.5 mL microcentrifuge tubes. These tubes were then subjected to centrifugation at 22,000 g for 10 minutes at 4 ºC. After the completion of centrifugation, the supernatant was removed, and the myelin pellet was weighed. To create a control sample consisting of non-oxidized myelin debris, the pellet from half of the tubes was diluted to a concentration of 100 mg/mL using HBSS solution. On the other hand, to generate oxidized myelin debris, the remaining tubes were resuspended using 50 µL of CuH (800 µM), $CuSO_4 \cdot 6H_2O$, and 20 mM H_2O_2. Following an incubation period of 16 hours at 37 ºC, the tubes were subjected to another round of centrifugation at 22,000 x g for 10 minutes at 4 ºC. The resulting pellet was then resuspended using HBSS solution to achieve a final concentration of 100 mg/mL.

4.2.2 Labeling of Myelin Debris

The fluorescent dye carboxyfluorescein succinimidyl ester (CFSE) was used to label the myelin debris. This dye has a non-cytotoxic nature, allowing for the monitoring of myelin debris internalization by the BV-2 cells following treatment. Furthermore, CFSE exhibits a narrow fluorescent spectrum, facilitating its simultaneous use with other fluorescence assays. For labeling, a 50 µM CFSE solution was prepared immediately before use, using HBSS to dilute the stock solution.

The myelin debris, previously obtained at a concentration of 100 mg/mL (oxidized and non-oxidized), was transferred to a pre-weighed 1.5 mL microcentrifuge tube. The tube was then centrifuged for 10 minutes at 4°C and 14,800 x g. After discarding the supernatant, the resulting pellet containing the myelin debris was resuspended using 200 µL of CFSE solution for every 100 µL of pellet. The mixture was incubated for 30 minutes at room temperature, protected from light exposure. Following this incubation period, the tube was once again centrifuged under the same conditions, and the supernatant was discarded once again. To cleanse the labeled debris, the pellet was resuspended in 600-800 µL of a wash buffer (100 mM glycine in HBSS). This centrifugation and washing process was repeated twice more. Finally, the weight of the myelin debris pellet was determined, and it was resuspended at a concentration of 100 mg/mL using sterile HBSS [21].

4.3 Cell Culture and Administration of Treatments

The BV-2 cell line was cultured in culture dishes with DMEM High Glucose medium supplemented with L-glutamine, pyruvate, fetal bovine serum, and antibiotic-antimycotic. Passages were performed every 2-3 days when confluence reached 70-80%. The incubator maintained a temperature of 37 ºC and a CO_2 concentration of 5%. For the treatments, 250,000 cells were seeded per well (in 1 mL of medium) in four plates with twelve wells each, using the same medium. The cells were allowed to grow for 2-3 days until reaching a confluence of 70-80%. Before applying the treatment, the medium was changed to DMEM High Glucose supplemented with L-glutamine, pyruvate, and antibiotic-antimycotic (without fetal bovine serum).If the myelin debris had been stored at-80 ºC, it was resuspended 4-5 times using a 0.5 x 16 mm needle and vigorously agitated before adding it to the cells.

Three plates followed the treatment scheme depicted in *Figure 3*, with the indicated amounts of myelin debris (whether oxidized or non-oxidized) at a concentration of 100 mg/mL. These plates were used for viability assays, protein quantification, and the study of proinflammatory cytokines. The last plate followed a different scheme, *Figure 4*, using control and oxidized myelin debris (100 mg/mL) that had been previously labeled with CFSE. The labeled myelin debris was applied at different time points for each row of wells (3, 6, and 24 hours).

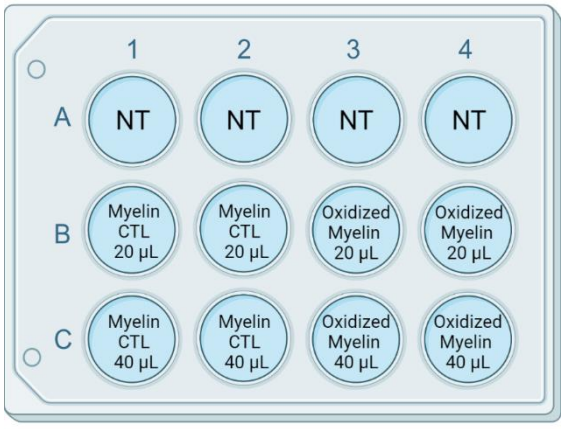

Figure 3. Treatment administration scheme in the twelve-well plate for viability assay, protein quantification, and proinflammatory cytokine assay.

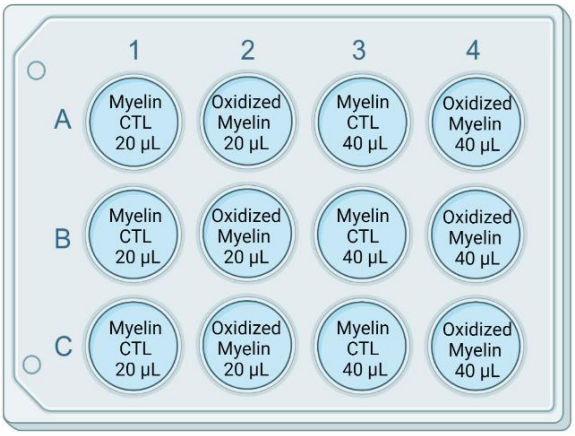

Figure 4. Treatment administration scheme in the twelve-well plate for assay with CFSE-labeled myelin debris.

4.4 Viability Assay

The viability study was conducted using one of the plates treated according to the *Figure 3* scheme. This was done using PrestoBlue reagent. PrestoBlue is a viability indicator that leverages the reducing capacity of alive cells metabolism to convert the non-fluorescent dye resazurin (with a blue color) into the fluorescent molecule resorufin (with a pink color). To prepare the PrestoBlue solution, 1 mL of the reagent was diluted in 12 mL of DMEM High Glucose medium supplemented with L-glutamine, pyruvate, and antibiotic-antimycotic. The medium in the plate was replaced with this solution, and then it was incubated for one hour in an incubator. After incubation, the fluorescence was measured using a fluorescence-based microplate reader. Nine readings were taken for each well, and the average of these readings was calculated for further statistical analysis. The obtained averages were normalized using the average fluorescence of the untreated wells, and thus expressed as % NT (normalized to control). This entire process was repeated three times to ensure robustness and reliability of the results.

4.5 Protein Quantification

Firstly, the cells were harvested from the culture plate using a lysis buffer composed of RIPA. This specialized lysis buffer not only disrupts the cell membranes but also facilitates the isolation of proteins by effectively solubilizing and stabilizing them, preventing degradation. To further preserve the protein, the RIPA buffer was supplemented with protease inhibitors and Na_3VO_4, and NaF, which are phosphatase inhibitors.

The cells were initially washed with HBSS, followed by the addition of 100 µL of the aforementioned lysis buffer. Using a cell scraper, the adherent cells were gently detached and collected in 1.5 mL tubes placed on ice. To further assist in the protein extraction, the samples were then subjected to sonication for thirty seconds at an amplitude of 10%. After extraction, the protein content in each sample was quantified using the Bradford protein assay. The samples were subsequently prepared for Western blot analysis, enabling the specific quantification of target proteins (*Table 1)*. For the preparation of the loading buffer, the calculated amount of β-mercaptoethanol, a denaturing agent that reduces protein aggregation and facilitates migration, was added. Additionally, bromophenol blue was included in the buffer to visually monitor the progress of electrophoresis and protein migration. Tris-MOPS-SDS running buffer and SurePAGE™ precast gels (Bis-Tris, 10x8, 4-12%, 15 wells) were employed for electrophoresis.

Following electrophoresis, the proteins were transferred onto membranes, images were captured using the ChemiDoc XRS+ System, and subsequently stained with Coomassie membrane stain.

Band intensities were quantified using the ImageLab software, and the values were normalized based on the protein quantification obtained from the membrane stain. The normalized values were expressed as % NT (normalized to control), using the average of the NT values as the reference set at 100%. The entire process was repeated four times to ensure the robustness and reliability of the results.

Table 1. Antibodies used for protein quantification using the Western Blot method.

Protein	Dilution	Reference	Secondary Ab	kDa
Sod2	1:1000	AB_2787145	Mouse	20
P-Erk	1:1000	AB_2809161	Rabbit	42-44
Erk ½ total	1:1000	AB_ 184699	Rabbit	42-44
Catalase	1:1000	AN_16731	Rabbit	60
Cleaved caspase 3	1:1000	ASP175	Rabbit	32
Gpx4	1:1000	67763-1-Ig ProteinTech	Mouse	20
Tfr1	1:500	AB_2533029 ThermoFisher	Mouse	84
Acsl4	1:1000	Abcam (Ab 155282)	Rabbit	75
p62	1:1000	5114 (Cell signaling)	Rabbit	62
Lc3b	1:1000	2775 (Cell signaling)	Rabbit	14-18

4.6 Study of Proinflammatory Cytokines

One of the 12-well plates treated according to the *Figure 3* scheme was selected. Initially, two washes were performed using HBSS, followed by the addition of 500 µL of TRIzol. This reagent dissolves the cell membranes, lysing the cells and releasing the intracellular contents, including RNA. The contents of the wells were collected in pre-labeled 2 mL tubes, and 100 µL of chloroform was then added. After agitation, the mixture was left to settle at room temperature for five minutes and then centrifuged at 13,000 rpm for fifteen minutes at 4 °C. This centrifugation step facilitates phase separation, where the RNA is separated in the upper (aqueous) phase. The upper phase was carefully collected and transferred to 1.5 mL tubes, to which 250 µL of isopropanol was added. After vortexing, the mixture was left to rest for 10 minutes at room temperature and then centrifuged at 13,000 rpm for ten minutes at 4 °C. The purpose of isopropanol is to precipitate the RNA, and therefore, the supernatant was discarded. Next, 500 µL of 75% ethanol (in H_20 RNAse-free) was added to the pellet, followed by vortexing and centrifugation for five minutes at 13,000 rpm at 4 °C. This washing step helps eliminate impurities, contaminants, and residual salts from the sample. The ethanol was carefully removed, and after allowing it to evaporate for a few minutes, the RNA was resuspended in 20 µL of RNAse-free water. Once the RNA was isolated, a microvolume spectrophotometer was used to quantify the RNA content in each sample and

detect possible contaminations. The samples were then diluted to a concentration of 1 µg/µL in a final volume of 10 µL using RNAse-free water.

The expression of proinflammatory cytokines (TNF-α, IL-1a, and IL-6) and actin as a reference gene was studied. Reverse transcription PCR (RT-PCR) was performed in order to obtain cDNA. This cDNA was then used in a quantitative PCR (qPCR) using SYBR Green. The SYBR Green dye binds to the double-stranded DNA, increasing its fluorescence emission and allowing for quantification. Each sample was analyzed (with duplicates) on a 96-well plate. The results obtained from the qPCR were analyzed using qPCR Analysis Software (CFX Maestro Software for Bio-Rad CFX Real-Time PCR Systems). The cycle threshold (Ct) values were obtained, which represent the number of amplification cycles required for the fluorescence signal to reach a detectable threshold. The relative expression of the target genes (TNF-α, IL-1a, and IL-6) was calculated using the $2^{-\Delta Ct}$ formula, where ΔCt is the difference between the Ct values of the target gene and the reference gene, actin. This expression was presented as %NT, with 100% representing the average of the NT values. This entire process was repeated a total of three times.

4.7 CFSE Assay

This twelve-well plate is treated following the scheme shown in *Figure 4*. The three rows need to be treated at separate times. First, the bottom row (C, 24 h) is treated with CFSE-labeled oxidized and control (CTL) myelin debris. After 18 hours, the middle row (B, 6 h) is treated, followed by the top row (A, 3 h). The cells are then fixed by adding 1 mL of 4% paraformaldehyde to each well and incubating at room temperature for 30 minutes. Since CFSE allows simultaneous staining with other dyes, a staining with DAPI is performed. The cells are washed 1-3 times with HBSS and then covered with a sufficient amount of DAPI staining solution (300 nM). After incubating for 1-5 minutes, protected from light, the cells are washed again.

Next, the cells are visualized using a fluorescence microscope. Considering the excitation/emission wavelengths of 358/461 nm for DAPI and 492/517 nm for CFSE, images are taken at ten distinct positions within each well, capturing three images for each position: DAPI fluorescence, CFSE fluorescence, and a phase-contrast image. The NT wells from the other procedures are also observed to ensure there is no fluorescence in them. The obtained images are analyzed using the Cell Profiler software. A pipeline is created, utilizing the nuclei detected by DAPI fluorescence to locate the cells. Phagosomes are also identified, and the RelateObjects module is used to identify intracellular phagosomes. Modules are developed to count these intracellular phagosomes, measure their area, perimeter, and eccentricity, and analyze the fluorescence intensity of CFSE-labeled myelin. This provides results on a per-cell basis.

For the myelin intensity analysis, ten values corresponding to the average intensity of each CFSE image are obtained for each condition and time point. Regarding perimeter and area measurements, the values are initially in pixels. To convert them to nanometers (nm), an image with a known scale in nm, captured under the same microscope and objective conditions, is used. This conversion is applied to both perimeter and area values.

4.8 TBARS Assay

To evaluate the success of the myelin debris oxidation, a thiobarbituric acid reactive substances assay (TBARS assay) was conducted. This assay is based on the principle that peroxidation processes generate various byproducts, including malondialdehyde (MDA) as a secondary product. MDA reacts with thiobarbituric acid (TBA) to form MDA-TBA2, a conjugate that exhibits absorption in the visible spectrum at 532 nm. This results in a distinctive rosy coloration, serving as a reliable indicator of the oxidation levels present in the sample.

The TBARS assay was performed following the specific protocol outlined in [22], First, the reagents were prepared. A 3.5 M sodium acetate buffer was prepared by diluting 200 mL of glacial acetic acid in 350 mL of ddH_2O. Separately, 50 mL of a 6.5 M NaOH solution was prepared, and 46 mL of this solution was slowly added to the acetic acid while continuously mixing it. The pH was adjusted to 4, and the solution was brought to a total volume of 500 mL with ddH_2O.

The other reagents prepared were: 4 mL of an 8.1% sodium dodecyl sulfate (SDS) solution in ddH_2O, 20 mL of a 5 M NaOH solution, and 100 mL of a 0.8% aqueous solution of thiobarbituric acid (TBA). To ensure smooth dissolution of the TBA in the last solution, 600 µL of the 5 M NaOH solution was gradually added in 100 µL increments until the TBA was completely dissolved. The pH was then adjusted to be below 4. To prepare the MDA standards, 9.2 µL of tetramethoxypropane malonaldehyde bis was added to 100 mL of ddH_2O, resulting in a final concentration of 550 µM. From this solution, standards at concentrations of 200, 100, 80, 40, 20, 10, 5, and 2.5 µM were prepared.

For the TBARS assay, 25 µL of the standard solutions were added to 2 mL tubes. For the samples, 12.5 µL of oxidized and control myelin debris, as well as 12.5 µL of ddH_2O, were added to 2 mL tubes. To each tube, 50 µL of the 8.1% SDS solution, 375 µL of the 3.5 M sodium acetate buffer, and 375 µL of the 0.8% TBA solution were added. The tubes were vortexed and incubated for 1 hour at 95 °C. Afterward, the tubes were cooled for 30 minutes on ice and centrifuged at 3,700 RPM for 10 minutes at 4 °C. 150 µL of the supernatant from each sample/standard was transferred

to separate wells in a 96-well plate (three wells per sample). In conclusion, the spectrophotometer was utilized to measure the absorbance at 532 nm. A standard curve was created using the absorbance values of the standards, and its equation was used to extrapolate the MDA concentration of the myelin debris samples. This extrapolation will provide information about the extent of lipid peroxidation in the control and oxidized myelin debris.

4.9 Statistical Analysis

All statistical analyses were conducted using GraphPad Prism 8.0.2 software.

The statistical analysis of the viability assay, protein quantification, and proinflammatory cytokine studies were subjected by comparison of the %NT (normalized values) obtained from the different treatment groups using a one-way ANOVA, followed by Tukey's multiple comparison test to elucidate any significant differences among the groups. For the CFSE reagent assays, a comprehensive analysis was performed. The fluorescence intensity data, collected from 10 replicates encompassing various conditions and time points, underwent a two-way ANOVA. Subsequently, multiple comparisons were executed using Tukey's test. Given the large amount of data for area, perimeter, eccentricity, and intracellular phagosome counts, GraphPad software is employed to obtain sample size, mean, and standard deviation for each condition and time point. Statistical analysis is performed using a two-way ANOVA y multiple comparison con Tukey. In the case of the TBARS Assay the concentrations of MDA obtained from the three replicates of both control and oxidized myelin debris were subjected to statistical analysis using an unpaired Student's t-test conducted. This analysis allowed for the comparison and assessment of the significance between the groups.

5. RESULTS

5.1 Viability Assay

In relation to the viability assay, no statistically significant difference ($p > 0.05$) was detected between the untreated groups and the groups exposed to varying concentrations of control and oxidized myelin, thereby suggesting the maintenance of cellular viability across all experimental conditions. The findings, illustrating these outcomes, are graphically presented in *Figure 5*.

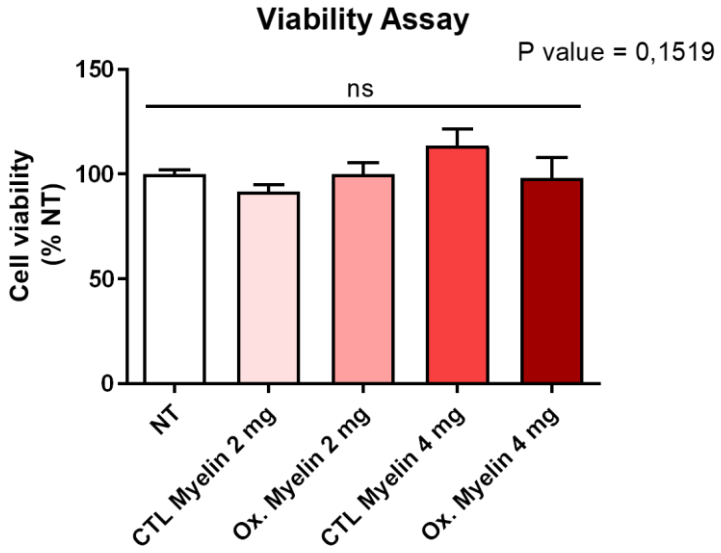

Figure 5. Bar graph resulting from the One-Way ANOVA analysis of the viability of the distinct groups, expressed as a percentage relative to the average viability calculated in the no treatment groups (%NT). NT (non-treatment), CTL (control), Ox. (Oxidized), ns (non-significant).

5.2 Oxidation Of Myelin

The degree of oxidation of the oxidized myelin was evaluated for the experiment, contrasting it with the level of oxidation of the control myelin, using the TBARS assay. The obtained data revealed a statistically significant distinction ($p < 0.01$), as depicted in *Figure 6. A* Consistent with expectations, the degree of oxidation in the oxidized myelin was notably higher than that observed in the control myelin. Visual inspection of the myelin samples in *Figure 6. B* further substantiates this contrast, wherein the oxidized myelin exhibits a distinct brown coloration, while the control myelin displays a whitish hue. To investigate the fluorescence emissions, an image (*Figure 6. C*) was captured to compare the fluorescence emitted by the control myelin and the oxidized myelin against the background buffer (HBSS) used. Notably, owing to the inherent autofluorescence properties of myelin, discernible fluorescence signals were observed in the control myelin in contrast to the buffer alone. However, the autofluorescence from the oxidized myelin surpassed that of the control myelin, primarily attributable to the generation of conjugated bonds with delocalized electrons throughout the process of oxidation, leading to the emission of light within the fluorescence spectrum.

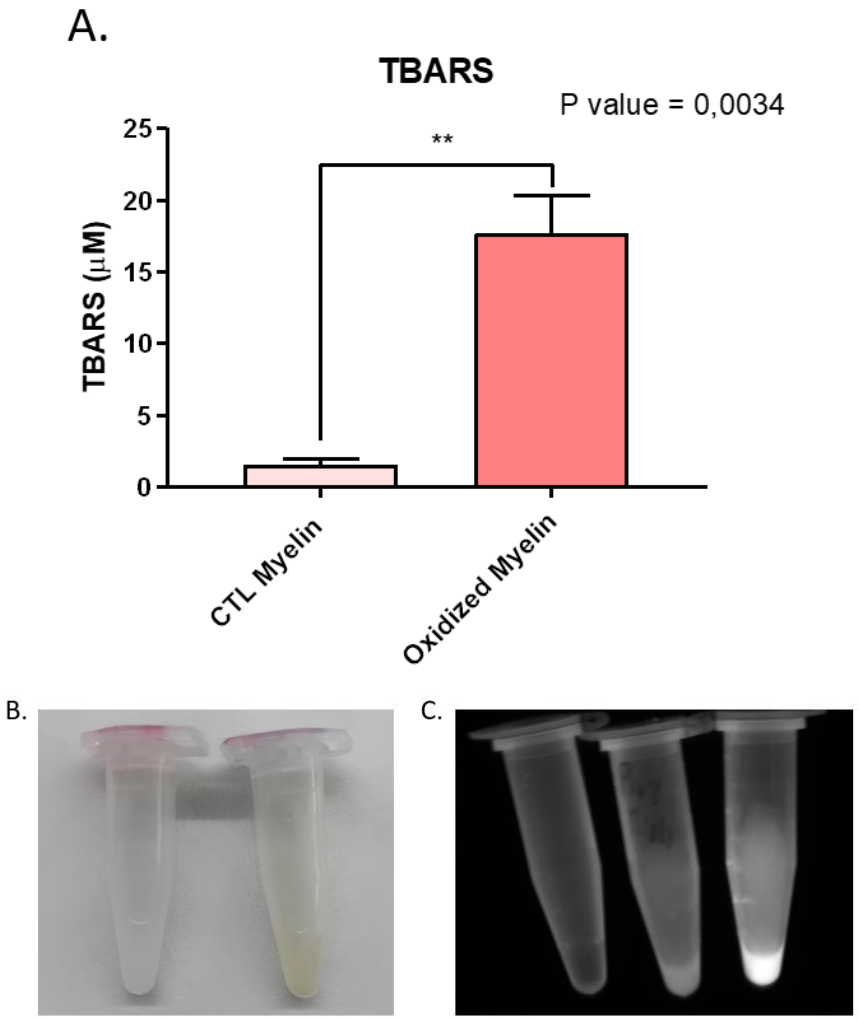

Figure 6. A. Displays the bar graph derived from the statistical analysis utilizing Student's t-test applied to the TBARS assay outcomes. The (**) indicate that the *p-value ≤ 0.01* **B.** An image depicting the control myelin samples (on the left) and oxidized myelin samples (on the right) at a concentration of 100 µg/µL. **C.** An image capturing the autofluorescence emitted by the samples, arranged from left to right: buffer, CTL myelin, and oxidized myelin. CTL (control), Ox. (Oxidized).

5.3 Protein Quantification

In the protein quantification via Western blot analysis, eleven distinct proteins of interest were examined. Following statistical analysis using one-way ANOVA, the only proteins that demonstrated significant differences among the treatment groups were: Superoxide Dismutase 2, Mitochondrial (Sod2, $p < 0.0001$), Transferrin Receptor Protein 1 (Tfr1, $p < 0.01$), p62, also known as sequestosome 1 ($p < 0.01$), and the ratio of Phosphorylated Extracellular-Signal-Regulated Kinase to total ERK (P-Erk/Erk total, $p < 0.05$).

Regarding Sod2, statistically significant differences were observed between all treatment groups and the untreated control group, with particularly notable distinctions between the no treatment (NT) group and Oxidized Myelin (2 mg), and between NT versus CTL Myelin (4 mg), both displaying a $p \leq 0.0001$. The next most significant comparison involving Sod2 was NT versus Oxidized Myelin

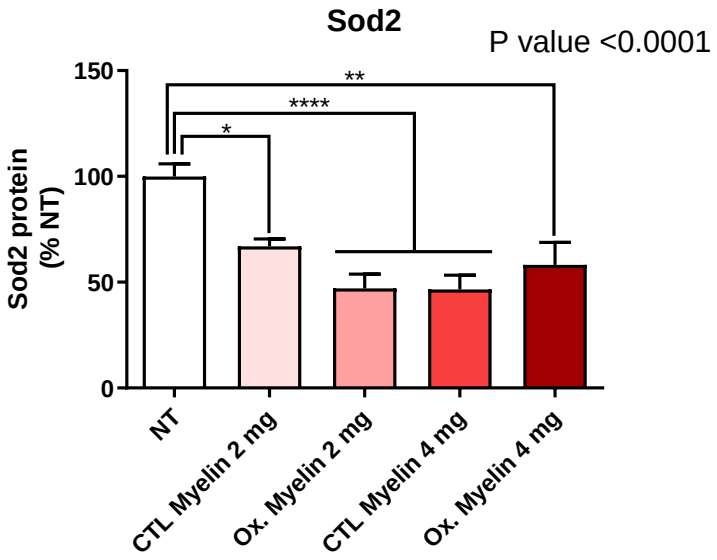

Figure 7. Superoxide Dismutase 2 (Sod2) protein quantification. The asterisks indicate significant values between the groups obtained from the Tukey test: (*) $p \leq 0.05$, (**) $p \leq 0.01$, and (****) $p \leq 0.0001$. The *p value* shown in the graph is the result of the one-way ANOVA. NT (non-treatment), CTL (control), Ox. (Oxidized).

(4 mg) with a $p \leq 0.01$, and finally NT versus Control Myelin (2 mg) with a $p \leq 0.05$. All treated groups exhibited lower Sod2 levels in contrast to the NT group, as illustrated in *Figure 7*.

In the case of Tfr1, significant differences were found in the comparisons between the NT group and CTL Myelin (4 mg) with a $p \leq 0.05$, as well as between the NT group and Oxidized Myelin (4 mg) with a $p \leq 0.01$. Both treated groups displayed higher levels of this protein in comparison to the untreated groups, as depicted in *Figure 8.*

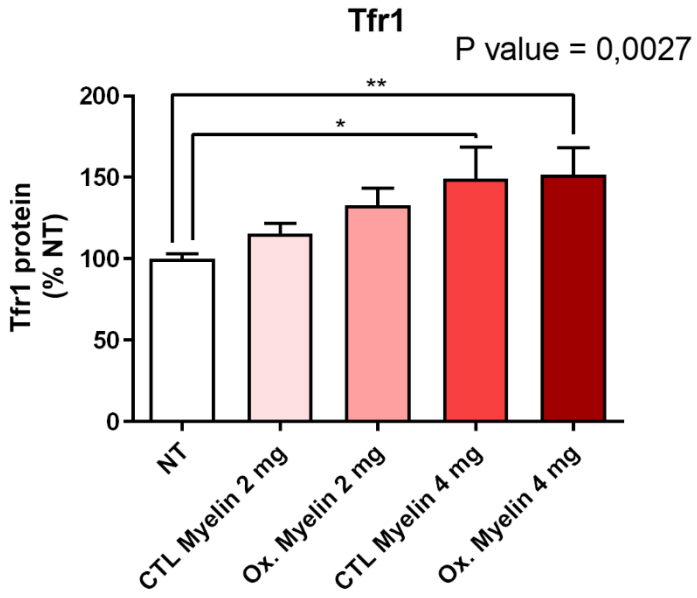

Figure 8. Transferrin Receptor Protein 1 (Tfr1) protein quantification. The asterisks indicate significant values between the groups obtained from the Tukey test: (*) $p \leq 0.05$, and (**) $p \leq 0.01$. The *p value* shown in the graph is the result of the one-way ANOVA. NT (non-treatment), CTL (control), Ox. (Oxidized).

For p62, all treated groups exhibited elevated levels of this autophagy protein relative to the NT group. However, only the NT group and Oxidized Myelin (4 mg) comparison yielded a significant *p-value* of ≤ 0.01. This is visually presented in the *Figure 9.*

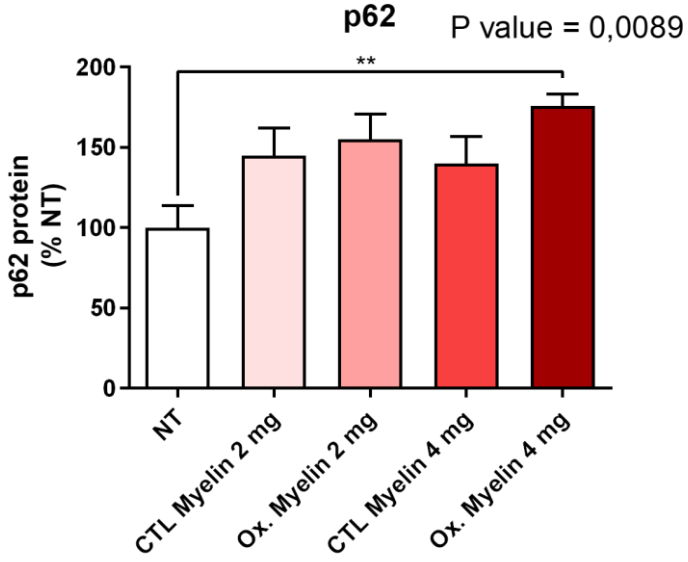

Figure 9. p62, also known as sequestosome 1, protein quantification. The asterisks indicate significant values between the groups obtained from the Tukey test: (**) $p \leq 0.01$. The *p value* shown in the graph is the result of the one-way ANOVA. NT (non-treatment), CTL (control), Ox. (Oxidized).

Finally, in relation to the P-Erk/Erk total ratio, a significant difference was observed between CTL Myelin (2 mg) and Oxidized Myelin (4 mg) with a $p \leq 0.05$. This indicates that the former displayed a lower ratio (and thus less phosphorylated Erk), while the latter exhibited a higher ratio (indicative of more P-Erk) in comparison to the average ratio of the NT group. These findings are graphically represented in the *Figure 10*.

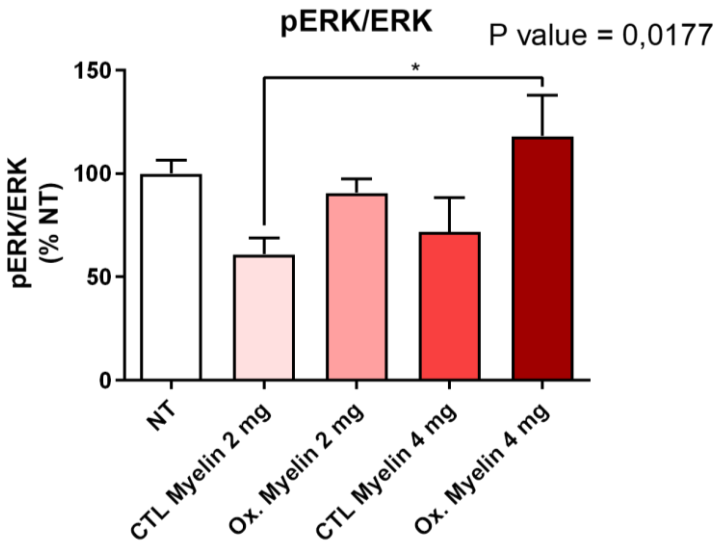

Figure 10. Phosphorylated Extracellular-Signal-Regulated Kinase to total ERK protein quantification ratio (P-Erk/Erk total). The asterisks indicate significant values between the groups obtained from the Tukey test: (*) $p \leq 0.05$. The *p value* shown in the graph is the result of the one-way ANOVA. NT (non-treatment), CTL (control), Ox. (Oxidized).

Figures presenting the statistical analysis for proteins that did not yield significant results can be found in the *Appendix* (*Figure 19*), alongside images of the conducted quantifications (*Figure 18*).

5.4 Study Of Proinflammatory Cytokines

After conducting a statistical analysis using One-way ANOVA on the three investigated cytokines, tumor necrosis factor-alpha (TNF-α) exhibited a *p-value* of 0.4245, interleukin 1 alpha (IL-1α) obtained a *p-value* of 0.1194, and interleukin 6 (IL-6) yielded a *p-value* of 0.2922. Based on these results, it was concluded that there were no statistically significant differences observed among the studied groups for these proinflammatory cytokines. For further elucidation, more detailed information can be found in the *Figure 11*

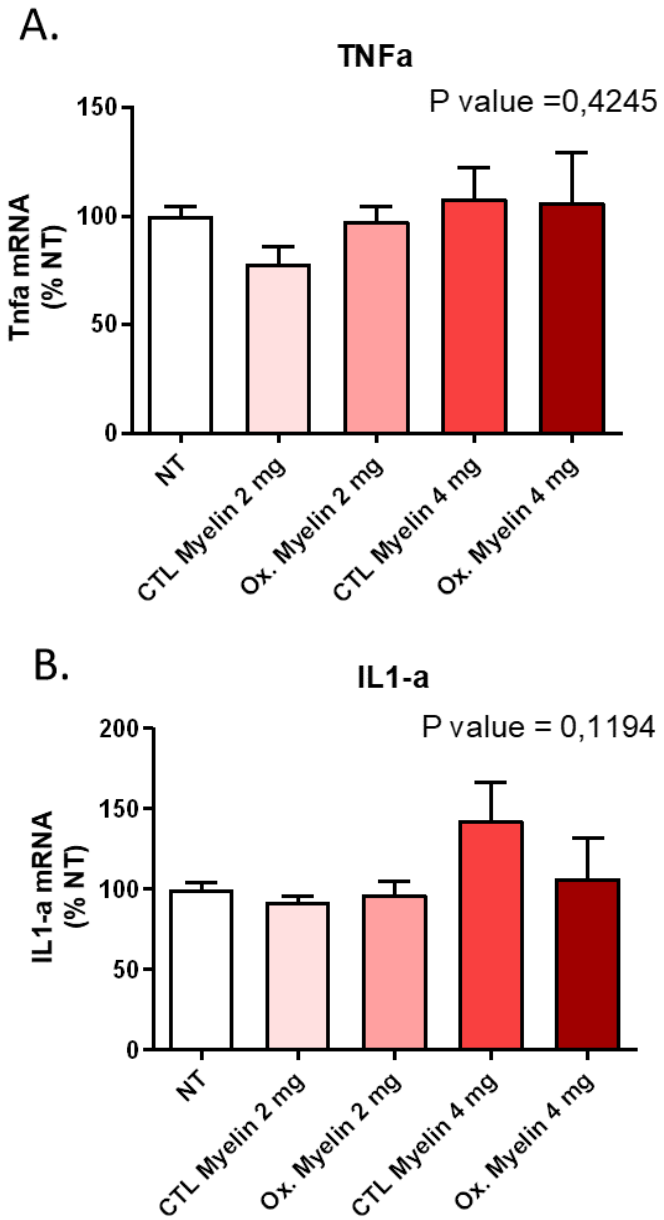

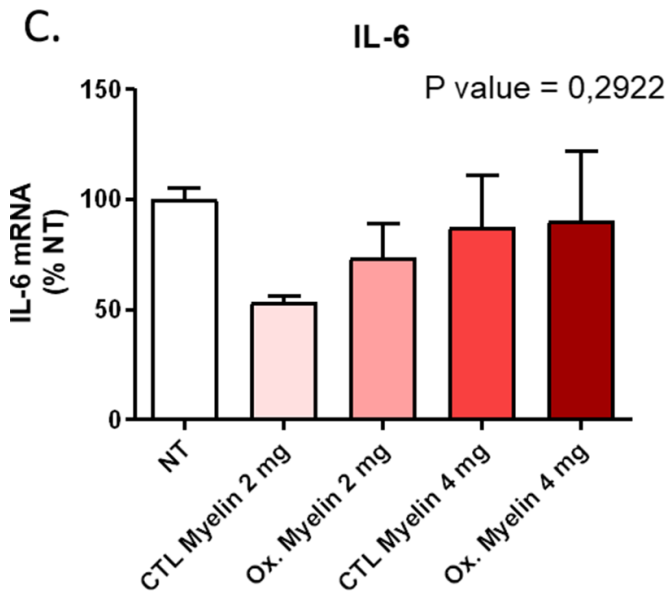

Figure 11. Expression of pro-inflammatory cytokines as a percentage relative to the mean of the untreated (NT) groups. **A.** Tumor necrosis factor-alpha (Tnf-a), **B**. Interleukin 1 a (IL-1a), and **C**. Interleukin 6 (IL-6). The *p value* shown in the graph is the result of the one-way ANOVA. NT (non-treatment), CTL (control), Ox. (Oxidized).

5.5 CFSE Assay

Remarkably, all the statistical analyses performed in the CFSE Assays yielded *p-values < 0.0001* for both the temporal and treatment factors, as well as their interaction, indicating an extremely significant disparity in the phagocytic characteristics of the treated BV-2 cells.

Concerning the number of intracellular phagosomes per cell (*figure 12),* it was discerned that following a 3-hour treatment, the cell population displayed less than 1 phagosome per cell, with higher quantities observed in cells subjected to elevated myelin doses (4 mg), particularly in the oxidized myelin group (4 mg). Analogously, at the 6-hour time point, a similar pattern emerged, exhibiting a substantial increase in the number of intracellular phagosomes within the CTL Myelin (4 mg) group. Subsequently, in the 24-hour treatment group, a notable trend alteration ensued, with a greater abundance of intracellular phagosomes observed in groups treated with oxidized myelin, exceeding 2 phagosomes per cell in the case of the oxidized myelin (4 mg) regimen. Conversely, the control myelin groups displayed a minimal increase (relative to the 6 hour one) when treated with both 2 and 4 mg myelin doses. In summary, the investigation revealed an augmented quantity of phagosomes within the cells following treatment with oxidized myelin, wherein the effect intensified with increasing myelin dosage and treatment duration. Conversely,

non-oxidized myelin demonstrated a more moderate alteration, which became more pronounced at higher concentrations, although not reaching the levels exhibited by the lower-concentration oxidized myelin.

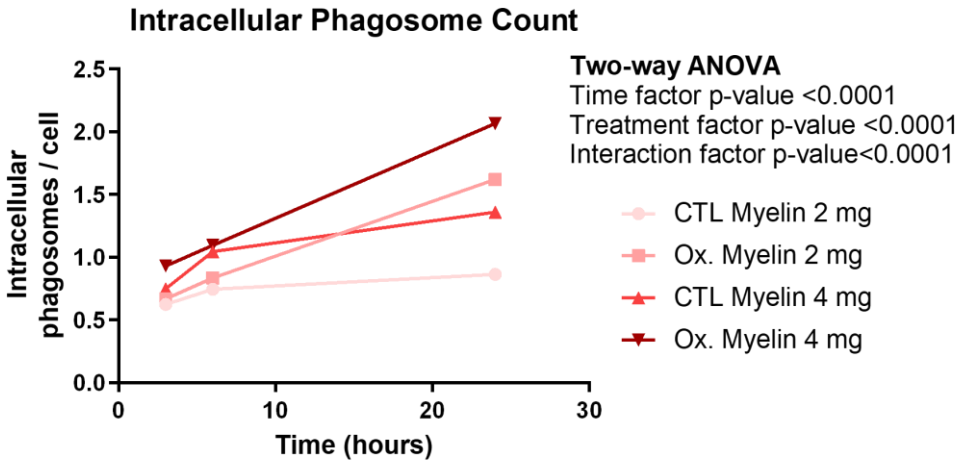

Figure 12. Number of myelin intracellular phagosomes per cell. The *p values* shown in the graph are the result of the two-way ANOVA. CTL (control), Ox. (Oxidized).

Evaluating the eccentricity (e) parameter to assess the shape of the phagosomes and their propensity for roundness, it was consistently observed that the eccentricity values surpassed 0.5 in all instances, indicating a lack of symmetry. The findings are illustrated in the *figure 13*. Specifically, during the 3-hour treatment, it became apparent that lower myelin doses (2 mg) for both oxidized and control myelin treatments yielded similar and lower eccentricity values, whereas higher myelin doses (4 mg) resulted in elevated eccentricity, particularly notable in the oxidized myelin (4 mg) group. However, at the 6-hour time point, this pattern shifted. Control myelin treatments exhibited a considerable increase in eccentricity compared to the previous time point, predominantly observed in the control myelin (4 mg) group, which surpassed the eccentricity of the oxidized myelin (4 mg) group. On the other hand, treatments with oxidized myelin demonstrated a slight elevation in eccentricity compared to the preceding time point, with a more significant alteration observed in the 2 mg oxidized myelin treatment. Lastly, after a 24-hour treatment, the eccentricity of phagosomes within groups subjected to higher myelin doses (both oxidized and non-oxidized) escalated to the point of nearly equalizing. Regarding the eccentricity resulting from the 2 mg treatments, the control myelin treatment exhibited a marginal increase compared to the previous time point, while the oxidized myelin treatment displayed a noteworthy elevation, almost reaching a comparable level of eccentricity. To

summarize, the administered myelin dose prominently influenced phagosome eccentricity, with higher quantities leading to greater eccentricity and consequently reducing phagosomal symmetry. Furthermore, a distinct divergence was observed between the oxidized myelin-treated groups and the control groups. The trend line for the oxidized myelin groups exhibited a consistently ascending trajectory across different time points. In contrast, the control myelin groups displayed a substantial surge from 3 to 6 hours, followed by a relatively modest increase at the 24-hour mark.

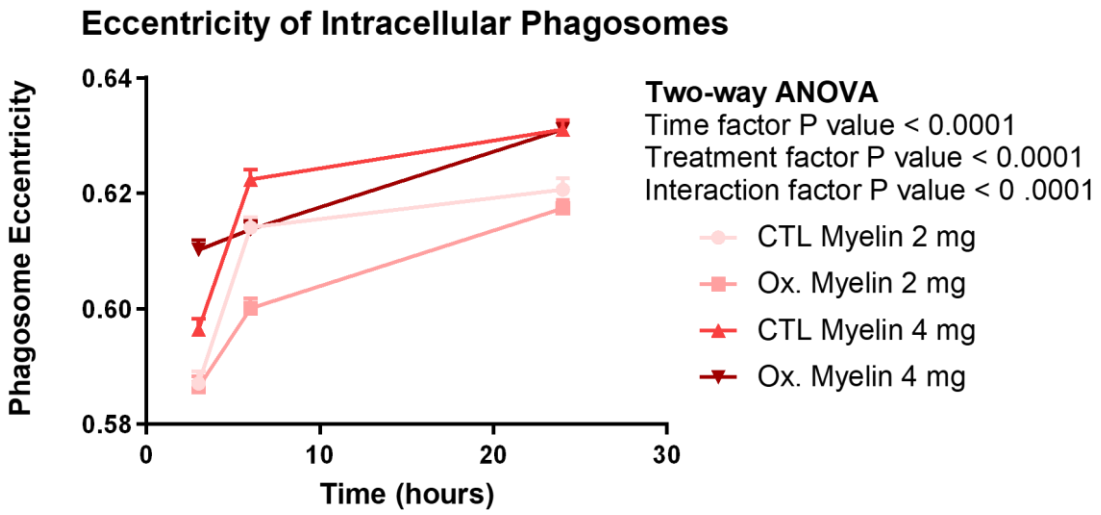

Figure 13. Eccentricity of the myelin intracellular phagosomes. The *p values* shown in the graph are the result of the two-way ANOVA. CTL (control), Ox. (Oxidized).

If we examine the perimeter of intracellular phagosomes (as illustrated in *figure 14*), it becomes evident that, from the outset, the intracellular phagosomes of myelin-treated cells exhibit a greater perimeter compared to those in the control myelin groups, at the initial time point examined (3 h). In the case of oxidized myelin, the perimeter is larger when subjected to a 4 mg dosage as opposed to a 2 mg dosage, while in the case of control myelin, the reverse is observed, with a larger perimeter noted in the 2 mg treatment compared to the 4 mg treatment. This trend of larger phagosomal perimeters in the groups treated with oxidized myelin persists at 6 hours. However, now, both control myelin and oxidized myelin groups display larger perimeters in the phagosomes resulting from treatments with a lower dosage (2 mg) compared to those with a higher dosage (4 mg) of the same myelin type (oxidized or control). Particularly intriguing is the case of oxidized myelin at 4 mg, which exhibits a reduction in perimeter when contrasted with its measurement at 3 hours. When shifting our focus to the 24-hour treatment, it becomes apparent that in the groups treated with control myelin, the phagosomes have undergone a drastic reduction in perimeter in both instances (2 mg and 4 mg), ultimately reaching an equivalent size. In contrast, within the group treated with oxidized myelin, the phagosomes subjected to the 2 mg

treatment demonstrate a slight decrease in perimeter compared to the previous time point, while those in the 4 mg treatment experience a significant increase in perimeter.

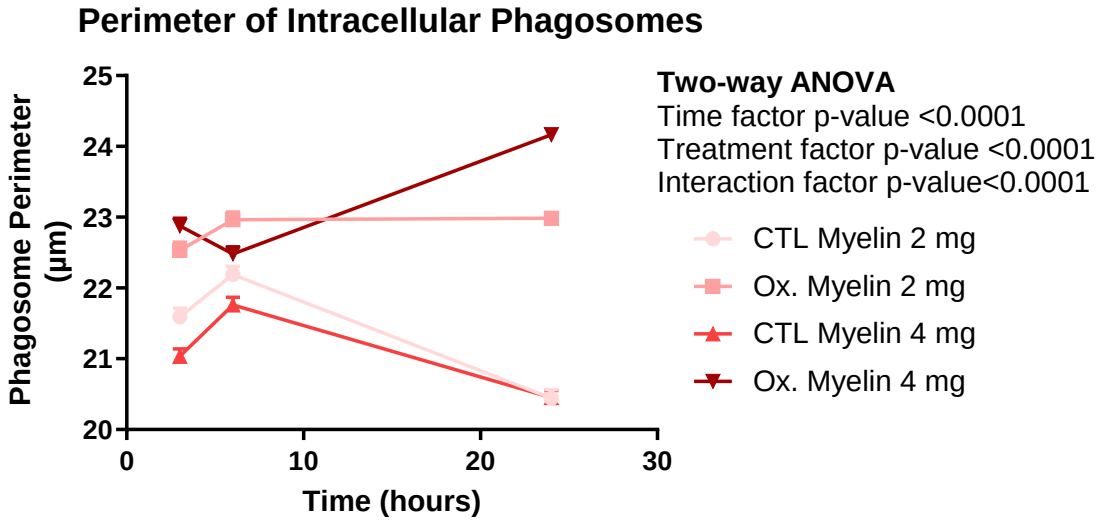

Figure 14. Perimeter in µm of the myelin intracellular phagosomes. The *p values* shown in the graph are the result of the two-way ANOVA. CTL (control), Ox. (Oxidized).

Upon examining the area (as illustrated in the *figure 15*), two distinct trends emerge. Three of the groups (CTL Myelin 2 mg, CTL Myelin 4 mg, and oxidized myelin 2 mg) display an increase in phagosomal area from 3 to 6 hours, followed by a subsequent decrease in this area (from 6 to 24 hours). In contrast, the area of intracellular phagosomes subjected to the oxidized myelin 4 mg treatment experiences a decrease from 3 to 6 hours, subsequently followed by a significant increase (6 to 24 h). This pattern aligns consistently with previous observations made during the analysis of perimeter (*Figure 14*). Specifically, at 3 hours, the phagosomal area in cells treated with oxidized myelin is practically identical, while in the case of control myelin treatment, the area is greater when a lower dosage of myelin (2 mg) is administered compared to a higher dosage (4 mg). Once again, at 6 hours, it can be observed that in treatments involving oxidized myelin, the area consistently exceeds that of the control groups across all time points, with the exception of the area of phagosomes in the CTL Myelin 2 mg treatment equaling that of the phagosomes in the oxidized myelin 4 mg treatment. It is notable that at 24 hours, the area of intracellular phagosomes resulting from control myelin treatment (similarly observed in the perimeter analysis) undergoes a dramatic reduction, nearly aligning with the area of phagosomes in the oxidized myelin group. Conversely, in the case of oxidized myelin, the area of the oxidized myelin 4 mg treatment increases, surpassing that of the 2 mg treatment, while the latter experiences a decrease compared to the previous time point (6 h).

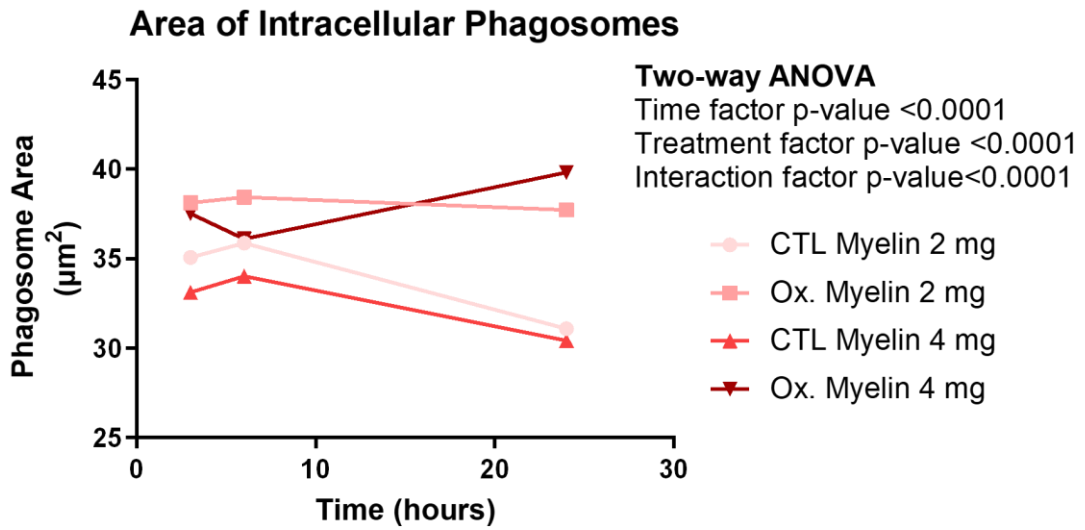

Figure 15. Area in µm^2 of the myelin intracellular phagosomes. The *p values* shown in the graph are the result of the two-way ANOVA. CTL (control), Ox. (Oxidized).

Finally, the analysis of fluorescence intensity of intracellular myelin, depicted in the *Figure 16*, revealed two distinct temporal trends based on the treatment groups. The oxidized myelin groups exhibited a consistent ascending pattern, wherein the fluorescence intensity progressively increased with longer treatment durations. In contrast, the control groups demonstrated a contrasting trend characterized by an initial increase in fluorescence from 3 to 6 hours, followed by a subsequent decrease at the 24-hour mark. This pattern closely resembled the observations made in the perimeter and area analyses. Notably, across all time points, the oxidized myelin 4 mg group consistently exhibited the highest fluorescence intensity.

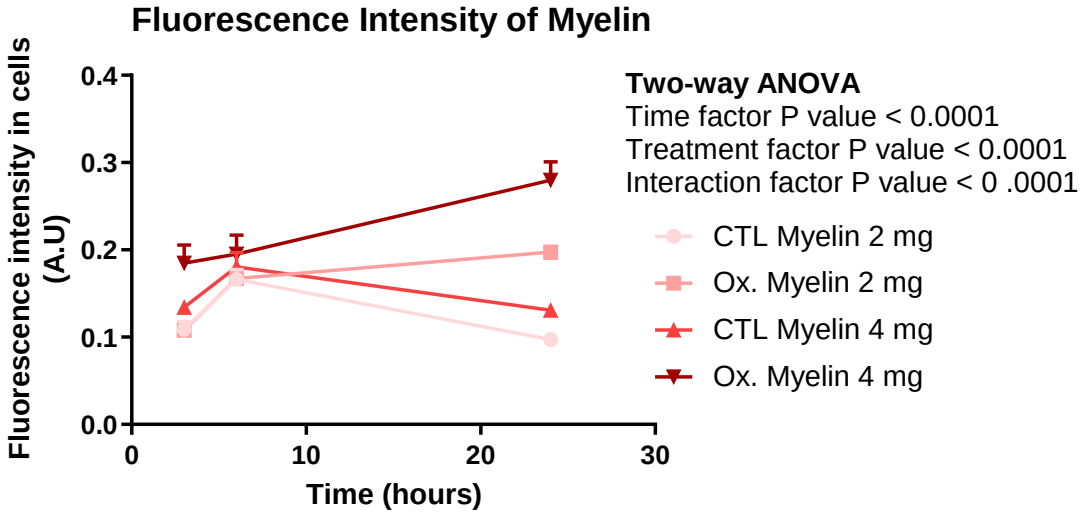

Figure 16. Fluorescence intensity of the different treatments and their duration with myelin (CTL and oxidized) labeled with CFSE. The *p values* shown in the graph are the result of the two-way ANOVA. CTL (control), Ox. (Oxidized).

The *Figure 17* presents a merged image composed of CFSE fluorescence and phase-contrast images. These images corresponded to different treatments administered at varying time points (3, 6, and 24 hours). The graphical representation depicted in the *Figure 16* aligns with the observed trends in the merged images, providing a clear visual confirmation. For a comprehensive evaluation, the supplementary material *Appendix* provides separate images (*Figure 20, 21, 22.*), including those of DAPI staining and the merge, for a thorough examination.

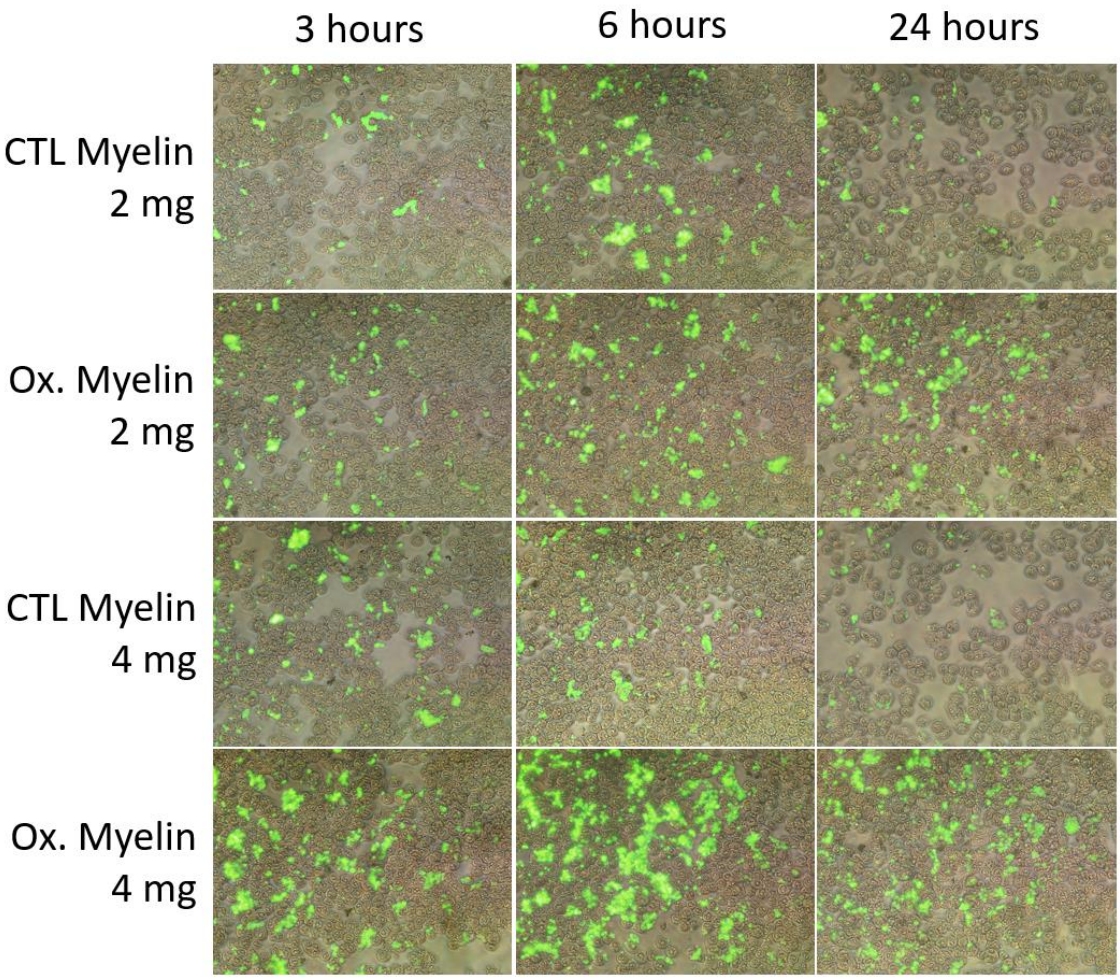

Figure 17. Merge of the images obtained from myelin fluorescence with phase-contrast images depicting the diverse treatments and administration durations. CTL (control), Ox. (Oxidized).

6. DISCUSSION

Given that MS is an autoimmune disorder characterized by the progressive destruction of myelin sheaths, the resultant accumulation of myelin debris necessitates efficient clearance mechanisms. In this context, the microglia emerge as a pivotal player, owing to its remarkable phagocytic activity and its capacity to phagocytose myelin debris. Given the inherent oxidative milieu characteristic of MS lesions and the phagocytic role of microglia in clearing said myelin debris, it

is hypothesized that the debris undergoes partial or complete oxidation. It is crucial, therefore, to comprehend how the oxidized state of myelin, which is phagocytosed by microglia, can influence the functional dynamics of these cells, potentially leading to unfavorable consequences that may exacerbate the pathological state in MS lesions. Hence, the primary objective of this study is to examine the impact of the aforementioned oxidized myelin on microglial cells. This investigation encompasses comprehensive evaluations, including the assessment of cell viability, quantification of proteins pertaining to diverse facets of cellular metabolism, and exploration of the expression of proinflammatory cytokines. Perhaps most interestingly and yielding the most significant results is the examination of intracellular phagosomes derived from the internalization of myelin debris by microglia and its correlation with the phagocytic capacity of said cells.

As stated in Results, no significant disparity in cellular viability was discerned upon. These findings align with the existing literature, as the pathological condition of oxidative injury characteristic of MS does not elicit cellular demise in microglia; rather, it induces a phenotypic transition towards a pro-inflammatory state [23]. Notably, the TBARS assay successfully confirmed the effective oxidation of myelin, affirming the suitability of the chosen oxidation protocol and rendering it an optimal model for investigating the impact of myelin oxidation in the context of MS.

The protein quantification analysis revealed substantial differences among the treated groups. Sod2 plays a pivotal role as a key metabolic component in regulating ROS within the mitochondrial matrix [24]. Oxidative stress denotes an imbalance between the production of oxidants, such as ROS, and the antioxidant capacity, which can induce detrimental effects on the biological system [25]. As previously mentioned, MS is characterized by lesions exhibiting elevated levels of ROS, leading to localized oxidative stress within the lesion site [12]. Across all treated groups, a significant reduction in Sod2 levels was observed compared to the NT group. This decline may be attributed to the phagocytic activity of microglia, which generates ROS and subsequently contributes to potential oxidative stress. The heightened ROS levels can deplete the cellular antioxidant capacity, including Sod2, consequently compromising the expression and activity of Sod2 and leading to decreased Sod2 levels [26]. During the phagocytosis of myelin, microglia have the ability to internalize iron from the breakdown products of myelin. This internalization process is facilitated by the Transferrin receptor protein 1 (Tfr1), which plays a crucial role in the import of iron through endocytosis. In the presence of H_2O_2, this iron can generate ROS through Fenton reactions [27]. The results of the quantification demonstrated that higher concentrations of oxidized myelin corresponded to elevated levels of Tfr1 compared to the control group. This observation is logical, given that greater quantities of myelin are associated with a higher iron content, leading to its accumulation [27,28]. These findings lend support to the hypothesis that the oxidation of myelin debris generated during oxidative attacks may contribute to tissue injury

by promoting inflammation to a greater extent than non-oxidized myelin. P62 serves as a crucial mediator between the targeted protein destined for degradation and the components of the autophagic machinery [29]. In the context of MS, aberrant expression of autophagy-related markers has been observed in immune cells, thus indicating a perturbation in this intricate cellular process [30]. Notably, a substantial increase in p62 levels was observed in response to treatment with 4 mg oxidized myelin. These findings suggested that the oxidative state of the myelin debris promotes autophagic processes, likely as a consequence of heightened ROS levels. The last quantification with a significant p-value was the P-Erk/Erk ratio. Extracellular signal-regulated kinase (ERK) plays a crucial role in signal transduction. Its activation occurs through phosphorylation, resulting in the activation or suppression of specific genes. Active ERK (p-ERK) is closely associated with the activation of immune cells, as well as their migration and the regulation of the inflammatory response [31]. By analyzing the results obtained from the experiment, the P-Erk and Erk ratio can be studied. A significant difference was observed between the 2 mg control myelin and the 4 mg oxidized myelin. Specifically, the former exhibited lower Erk activation, while the latter demonstrated higher activation when compared to the NT group. This trend is consistent when evaluating the other groups studied, where control myelin treatments consistently displayed lower ERK activation, while oxidized myelin treatments showed higher activation. It is important to acknowledge the significant role of active, phosphorylated ERK in cellular proliferation, survival, and differentiation [31]. The observed higher activation of ERK in the treatments involving myelin debris suggests a potential induction of microglial cell proliferation by oxidized myelin debris, potentially facilitating the clearance of such debris.

In the assessment of pro-inflammatory cytokine expression, namely TNFa, IL-1a, and IL-6, no statistically significant disparities were observed among the treated groups. These findings imply that the administered treatments, within the confines of the experimental conditions employed, fail to elicit an inflammatory response in BV-2 cells. It is plausible that additional factors are required to instigate this pro-inflammatory cascade, such as cellular interactions with other immune constituents or the activation of pro-inflammatory signaling pathways. This observation potentially implies that the presence of myelin may be more closely linked to a reparative phenotype rather than an inflammatory one.

Regarding the quantification of intracellular phagosomes per cell, a proportional increase in phagosome numbers over time was observed in the groups treated with oxidized myelin debris. In contrast, the control myelin groups exhibited a slight and minimal increase in phagosome count after 6 hours. This consistent increment across all groups suggests continuous phagocytosis.

When comparing groups treated with the same amount of control myelin to the respective oxidized myelin group, it was noted that both groups treated with oxidized myelin groups displayed a higher number of intracellular phagosomes per cells over time. This indicates that myelin oxidation may lead to an internal accumulation of these phagosomes, possibly due to impaired degradation caused by altered mechanisms of phagosome clearance. The lower phagosome count in the respective control groups implies that cells have greater ease in assimilating and degrading phagosomes derived from control myelin.

When analyzing the eccentricity (e) of these intracellular phagosomes, it becomes evident that eccentricity is more closely associated with the administered myelin quantity rather than its state (oxidized or non-oxidized). Groups treated with oxidized myelin exhibited higher eccentricity values (indicating less symmetry) compared to the respective control groups. However, it is important to note that in all cases, longer treatment duration corresponded to increased eccentricity. In the context of phagocytosis, the continuous increase of eccentricity over time, may indicate an accumulation of immature phagosomes or alterations in fusion and degradation processes, potentially linked to a dysfunction in microglial capacity to effectively process phagocytosed myelin debris.

If we examine the perimeter and area, both exhibited a parallel progression and could serve as indicators of phagosomal size. After a 24-hour period, a pronounced reduction in phagosome size was evident in the control groups, whereas the size remained substantially elevated in the groups exposed to oxidized myelin.
The size observed in the control groups suggests that the phagosomes have undergone degradation, resulting in a decrease in size. Conversely, in the groups treated with oxidized myelin, this degradation process may be altered due to the oxidative state of the myelin, leading to a decline in degradation capacity. Hence, it can be postulated that myelin oxidation, as evidenced by the phagosome count, impairs cellular processing, perturbs microglial metabolism, and culminates in the accumulation of intracellular phagosomes, potentially leading to future complications.

Lastly, the fluorescence intensity observed in the distinct wells was quantified. Consistent with the findings in the phagosomal area and perimeter analysis, oxidized myelin demonstrated an upsurge in fluorescence intensity with prolonged treatment duration, whereas control myelin exhibited a decline in fluorescence. This discrepancy may be attributed to the ability of cells to degrade phagosomal contents in the case of control myelin, which subsequently leads to the

degradation of the CFSE reagent and a consequent reduction in fluorescence. However, as suggested earlier, in the context of oxidized myelin treatment, the lysosomal degradation process is altered due to the oxidized state of the myelin, resulting in internal phagosome accumulation and consequently an increase in fluorescence intensity, which remains unaltered due to the absence of degradation.

7. CONCLUSION

In conclusion, the results obtained from this study strongly indicate that the presence of oxidized myelin debris profoundly impacts the phagocytic capacity of microglia, as well as its innate metabolic processes. These findings provide compelling evidence of compromised phagosome degradation and perturbed antioxidant mechanisms. Given the crucial role of microglia in clearing myelin debris and their high production of ROS, it can be inferred that the presence of myelin debris in an oxidative environment (during the lesion) and its subsequent oxidation could worsen the beneficial performance of microglia and, therefore, negatively impact the disease development. These findings suggest that the BV-2 cell model is indeed relevant for studying MS and it could be used for future in vitro drug testing.

The research was conducted by utilizing the results obtained from the internship undertaken at the Biomedical Research Institute of Lleida, Dr. Pifarré Foundation (IRBLleida), under the expert supervision of Dr. Luis Brieva and Dr. Pascual Torres.

8. REFERENCES

1. Faissner, S., Plemel, J. R., Gold, R., & Yong, V. W. (2019). Progressive multiple sclerosis: from pathophysiology to therapeutic strategies. Nature reviews. Drug discovery, 18(12), 905–922. https://doi.org/10.1038/s41573-019-0035-2
2. Huang, W. J., Chen, W. W., & Zhang, X. (2017). Multiple sclerosis: Pathology, diagnosis and treatments. Experimental and therapeutic medicine, 13(6), 3163–3166. https://doi.org/10.3892/etm.2017.4410
3. Dighriri, I. M., Aldalbahi, A. A., Albeladi, F., Tahiri, A. A., Kinani, E. M., Almohsen, R. A., Alamoudi, N. H., Alanazi, A. A., Alkhamshi, S. J., Althomali, N. A., Alrubaiei, S. N., & Altowairqi, F. K. (2023). An Overview of the History, Pathophysiology, and Pharmacological Interventions of Multiple Sclerosis. Cureus, 15(1), e33242. https://doi.org/10.7759/cureus.33242
4. Klineova, S., & Lublin, F. D. (2018). Clinical Course of Multiple Sclerosis. Cold Spring Harbor perspectives in medicine, 8(9), a028928. https://doi.org/10.1101/cshperspect.a028928
5. Primary progressive MS (PPMS) Primary progressive MS (PPMS). (2023). Retrieved 20 May 2023, from https://www.nationalmssociety.org/What-is-MS/Types-of-MS/Primary-progressive-MS
6. Tipos de Esclerosis múltiple- Esclerosis Múltiple España. (2023). Retrieved 7 May 2023, from https://esclerosismultiple.com/esclerosis-multiple/tipos-de-esclerosis-multiple/
7. Cree, B. A. C., Arnold, D. L., Chataway, J., Chitnis, T., Fox, R. J., Pozo Ramajo, A., Murphy, N., & Lassmann, H. (2021). Secondary Progressive Multiple Sclerosis: New Insights. Neurology, 97(8), 378–388. https://doi.org/10.1212/WNL.0000000000012323

8. Thompson, A. J., Baranzini, S. E., Geurts, J., Hemmer, B., & Ciccarelli, O. (2018). Multiple sclerosis. Lancet (London, England), 391(10130), 1622–1636. https://doi.org/10.1016/S0140-6736(18)30481-1
9. Rodríguez Murúa, S., Farez, M. F., & Quintana, F. J. (2022). The Immune Response in Multiple Sclerosis. Annual review of pathology, 17, 121–139. https://doi.org/10.1146/annurev-pathol-052920-040318
10. Steinman L. (2014). Immunology of relapse and remission in multiple sclerosis. Annual review of immunology, 32, 257–281. https://doi.org/10.1146/annurev-immunol-032713-120227
11. van Langelaar, J., Rijvers, L., Smolders, J., & van Luijn, M. M. (2020). B and T Cells Driving Multiple Sclerosis: Identity, Mechanisms and Potential Triggers. Frontiers in immunology, 11, 760. https://doi.org/10.3389/fimmu.2020.00760
12. Ontaneda D. (2019). Progressive Multiple Sclerosis. Continuum (Minneapolis, Minn.), 25(3), 736–752. https://doi.org/10.1212/CON.0000000000000727
13. Mado, H., Adamczyk-Sowa, M., & Sowa, P. (2023). Role of Microglial Cells in the Pathophysiology of MS: Synergistic or Antagonistic? International Journal of Molecular Sciences, 24(3), 1861. https://doi.org/10.3390/ijms24031861
14. Multiple Sclerosis Multiple Sclerosis. (2023). Retrieved 23 May 2023, from https://www.ninds.nih.gov/health-information/disorders/multiple-sclerosis
15. Hodgens A, Sharman T. Corticosteroids. [Updated 2022 Jul 26]. In: StatPearls [Internet]. Treasure Island (FL): StatPearls Publishing; 2023 Jan-. Available from: https://www.ncbi.nlm.nih.gov/books/NBK554612/
16. Travers, B. S., Tsang, B. K., & Barton, J. L. (2022). Multiple sclerosis: Diagnosis, disease-modifying therapy and prognosis. Australian journal of general practice, 51(4), 199–206. https://doi.org/10.31128/AJGP-07-21-6103
17. Mitoxantrone (Novantrone®) | OncoLink. (2021). Retrieved 23 May 2023, from https://es.oncolink.org/tratamiento-del-cancer/oncolink-rx/mitoxantrone-novantrone-r
18. Borst, K., Dumas, A. A., & Prinz, M. (2021). Microglia: Immune and non-immune functions. Immunity, 54(10), 2194–2208. https://doi.org/10.1016/j.immuni.2021.09.014
19. Allende, M. L., Zhu, H., Kono, M., Hoachlander-Hobby, L. E., Huso, V. L., & Proia, R. L. (2021). Genetic defects in the sphingolipid degradation pathway and their effects on microglia in neurodegenerative disease. Cellular signalling, 78, 109879. https://doi.org/10.1016/j.cellsig.2020.109879
20. BV-2 Microglial Cells | AcceGen . (2023). Retrieved 13 May 2023, from https://www.accegen.com/product/bv-2-abc-tc212s/#:~:text=BV%2D2%20is%20a%20type,antigen%20at%20the%20surface%20level
21. Rolfe, A. J., Bosco, D. B., Broussard, E. N., & Ren, Y. (2017). In Vitro Phagocytosis of Myelin Debris by Bone Marrow-Derived Macrophages. Journal of visualized experiments : JoVE, (130), 56322. https://doi.org/10.3791/56322
22. Aguilar Diaz De Leon, J., & Borges, C. R. (2020). Evaluation of Oxidative Stress in Biological Samples Using the Thiobarbituric Acid Reactive Substances Assay. Journal of visualized experiments : JoVE, (159), 10.3791/61122. https://doi.org/10.3791/61122
23. van Olst, L., Rodriguez-Mogeda, C., Picon, C., Kiljan, S., James, R. E., Kamermans, A., van der Pol, S. M. A., Knoop, L., Michailidou, I., Drost, E., Franssen, M., Schenk, G. J., Geurts, J. J. G., Amor, S., Mazarakis, N. D., van Horssen, J., de Vries, H. E., Reynolds, R., & Witte, M. E. (2021). Meningeal inflammation in multiple sclerosis induces phenotypic changes in cortical microglia that differentially associate with neurodegeneration. Acta neuropathologica, 141(6), 881–899. https://doi.org/10.1007/s00401-021-02293-4

24. Palma, F. R., He, C., Danes, J. M., Paviani, V., Coelho, D. R., Gantner, B. N., & Bonini, M. G. (2020). Mitochondrial Superoxide Dismutase: What the Established, the Intriguing, and the Novel Reveal About a Key Cellular Redox Switch. Antioxidants & redox signaling, 32(10), 701–714. https://doi.org/10.1089/ars.2019.7962
25. Forman, H. J., & Zhang, H. (2021). Targeting oxidative stress in disease: promise and limitations of antioxidant therapy. Nature reviews. Drug discovery, 20(9), 689–709. https://doi.org/10.1038/s41573-021-00233-1
26. Wang, Y., Branicky, R., Noë, A., & Hekimi, S. (2018). Superoxide dismutases: Dual roles in controlling ROS damage and regulating ROS signaling. The Journal of cell biology, 217(6), 1915–1928. https://doi.org/10.1083/jcb.201708007
27. Vogt, A. S., Arsiwala, T., Mohsen, M., Vogel, M., Manolova, V., & Bachmann, M. F. (2021). On Iron Metabolism and Its Regulation. International journal of molecular sciences, 22(9), 4591. https://doi.org/10.3390/ijms22094591
28. Tacchini, L., Gammella, E., De Ponti, C., Recalcati, S., & Cairo, G. (2008). Role of HIF-1 and NF-kappaB transcription factors in the modulation of transferrin receptor by inflammatory and anti-inflammatory signals. The Journal of biological chemistry, 283(30), 20674–20686. https://doi.org/10.1074/jbc.M800365200
29. Liu, W. J., Ye, L., Huang, W. F., Guo, L. J., Xu, Z. G., Wu, H. L., Yang, C., & Liu, H. F. (2016). p62 links the autophagy pathway and the ubiqutin-proteasome system upon ubiquitinated protein degradation. Cellular & molecular biology letters, 21, 29. https://doi.org/10.1186/s11658-016-0031-z
30. Shen, D., Liu, K., Wang, H., & Wang, H. (2022). Autophagy modulation in multiple sclerosis and experimental autoimmune encephalomyelitis. Clinical and experimental immunology, 209(2), 140–150. https://doi.org/10.1093/cei/uxac017
31. Lu, N., & Malemud, C. J. (2019). Extracellular Signal-Regulated Kinase: A Regulator of Cell Growth, Inflammation, Chondrocyte and Bone Cell Receptor-Mediated Gene Expression. International journal of molecular sciences, 20(15), 3792. https://doi.org/10.3390/ijms20153792

9. APPENDIX

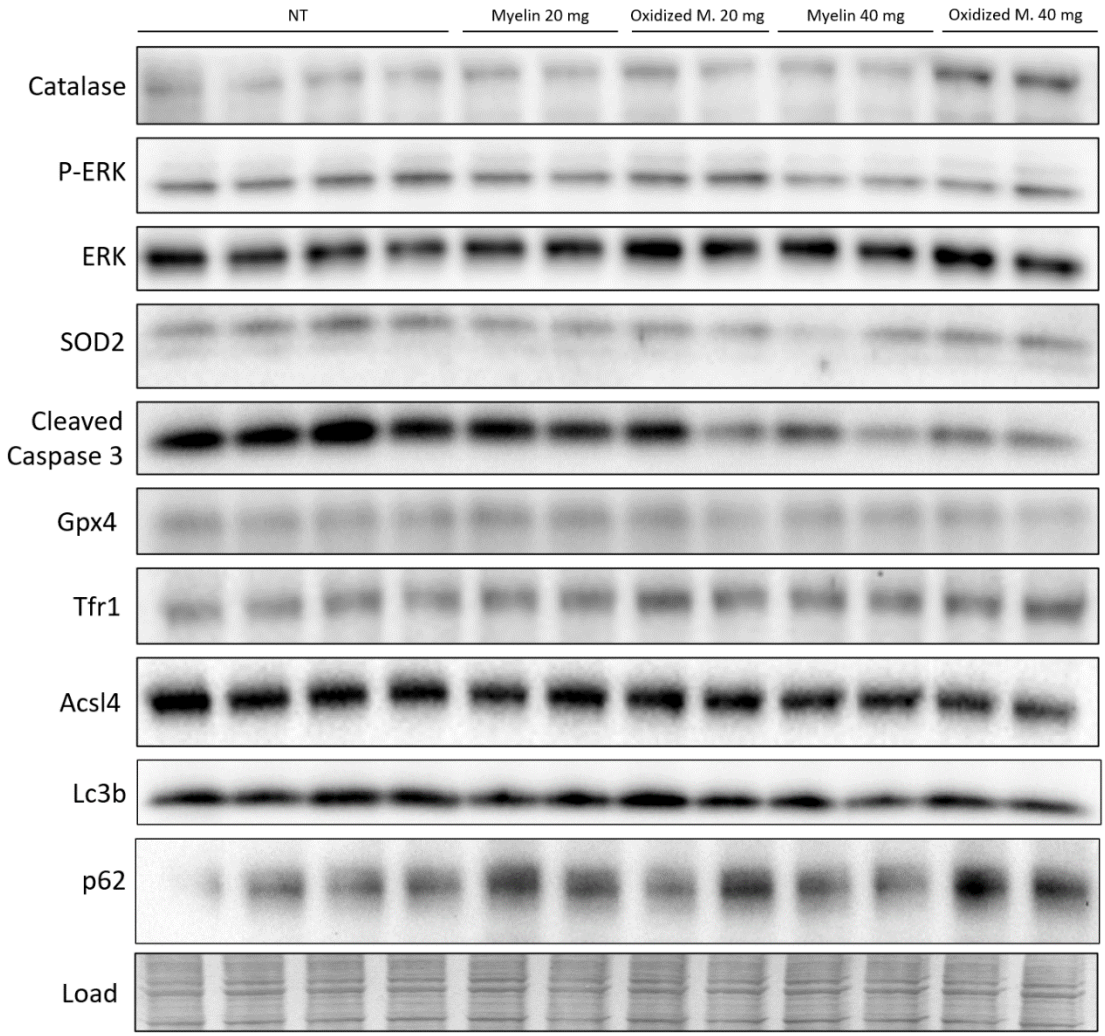

Figure 18. Compilation of the observed protein bands in one of the replicates of the Western blot for the protein quantification. The protein loading, visualized by staining the membranes with Coomassie, is shown at the bottom. The Coomassie-stained bands were used to determine the protein loading and normalize the quantification results.

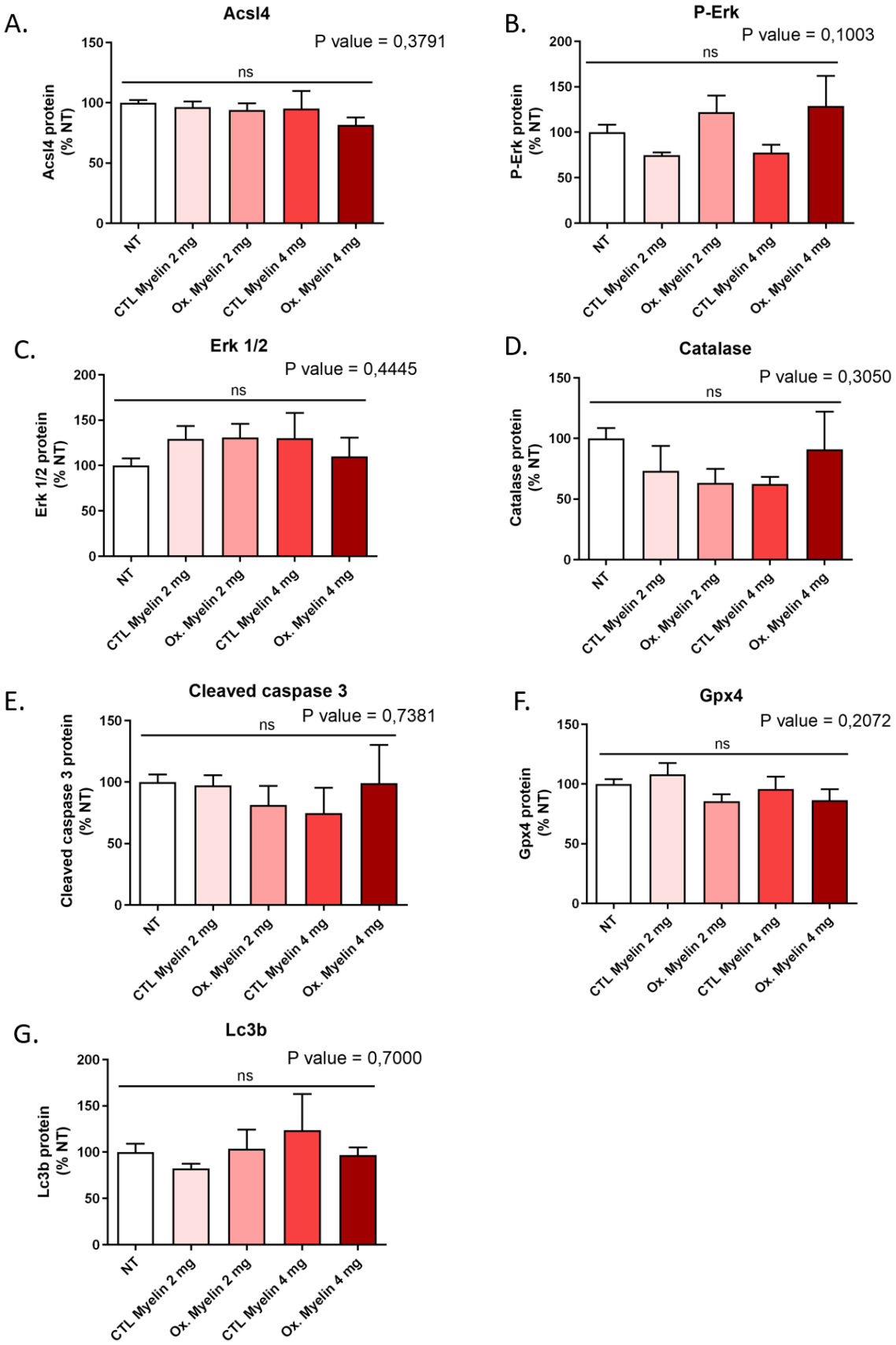

Figure 19. Protein quantifications that did not exhibit significant (ns) differences among the experimental groups. **A.** Acyl-CoA Synthetase Long-Chain 4 (Acsl4), **B.** P-Erk, **C.** Erk 1/2, **D.** Catalase, **E.** Cleaved caspase 3, **F.** Glutathione Peroxidase 4 (Gpx4) and **G.** Microtubule-associated Proteins 1A/1B Light Chain 3B (Lc3b). NT (non-treatment), CTL (control), Ox. (Oxidized), ns (non-significant).

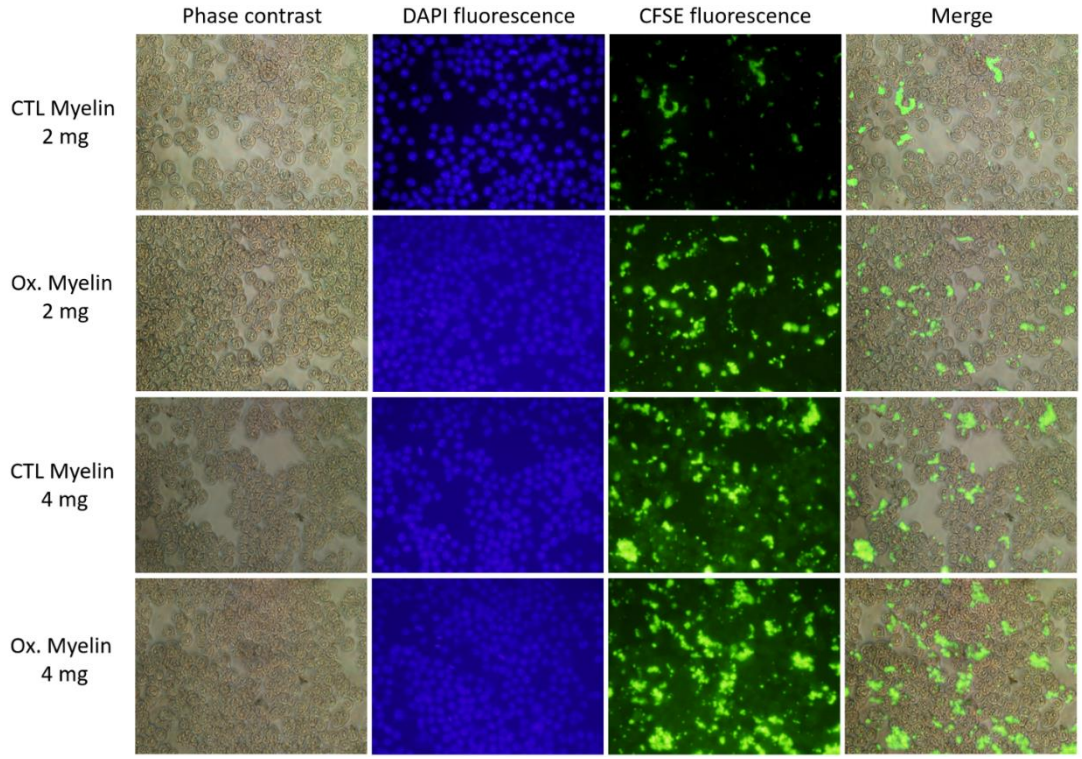

Figure 20. Images of the different treatments administered for 3 hours were captured through phase-contrast, DAPI fluorescence, CFSE fluorescence, and the merge of phase-contrast with CFSE

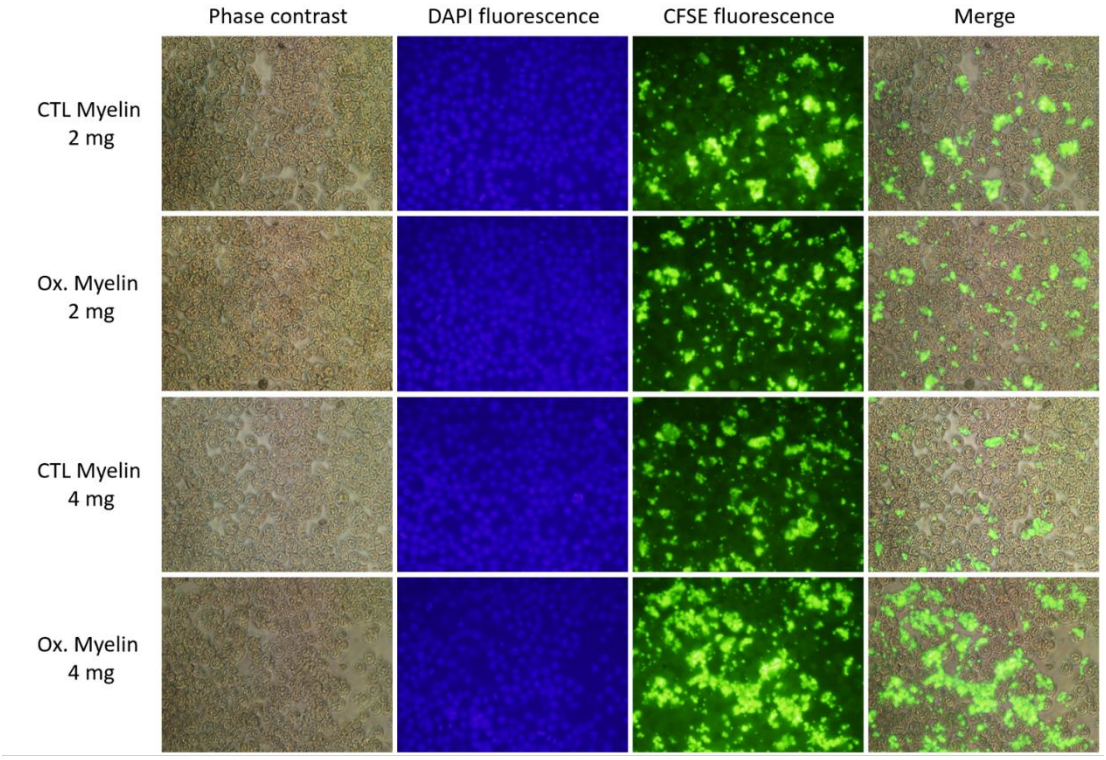

Figure 21. Images of the different treatments administered for 6 hours were captured through phase-contrast, DAPI fluorescence, CFSE fluorescence, and the merge of phase-contrast with

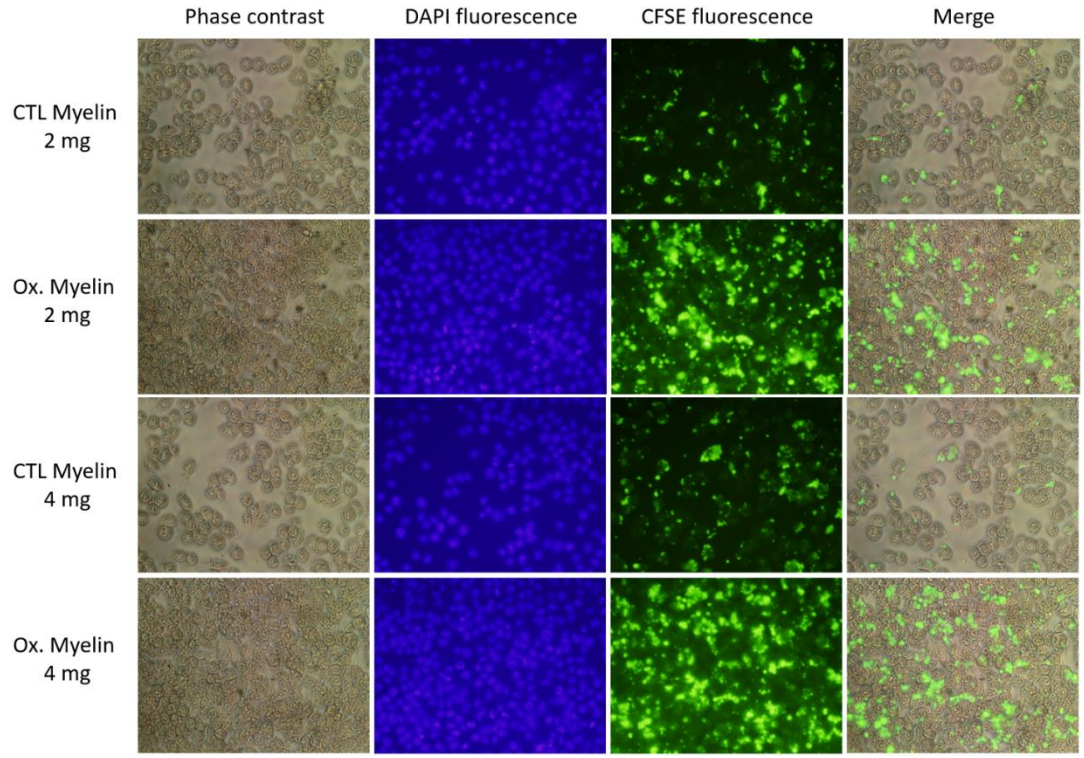

Figure 22. Images of the different treatments administered for 24 hours were captured through phase-contrast, DAPI fluorescence, CFSE fluorescence, and the merge of phase-contrast with